Validation of High Frequency Propagation Prediction Models over Africa

A thesis submitted in fulfillment of the
requirements for the degree of

MASTER OF SCIENCE

of

Rhodes University

by

Mpho Tshisaphungo

November 2009

Abstract

The ionosphere is an important factor in high frequency (HF) radio propagation providing an opportunity to study ionospheric variability as well as the space weather conditions under which HF communication can take place. This thesis presents the validation of HF propagation conditions for the Ionospheric Communication Enhanced Profile Analysis and Circuit (ICEPAC) and Advanced Stand Alone Prediction System (ASAPS) models over Africa by comparing predictions with the measured data obtained from the International Beacon Project (IBP). Since these models were not developed using information on the African region, a more accurate HF propagation prediction tool is required. Two IBP transmitter stations are considered, Ruaraka, Kenya (1.24°S, 36.88°E) and Pretoria, South Africa (25.45°S, 28.10°E) with one beacon receiver station located in Hermanus, South Africa (34.27°S, 19.12°E). The potential of these models in terms of HF propagation conditions is illustrated. An attempt to draw conclusions for future improvement of the models is also presented. Results show a low prediction accuracy for both ICEPAC and ASAPS models, although ICEPAC provided more accurate predictions for daily HF propagation conditions. This thesis suggests that the development of a new HF propagation prediction tool for the African region or the modification of one of the existing models to accommodate the African region, taking into account the importance of the African ionospheric region, should be considered as an option to ensure more accurate HF Propagation predictions over this region.

Acknowledgements

I am greatly honored by the Hermanus Magnetic Observatory (HMO) for the financial support to pursue my studies.

I would like to express my gratitude and appreciation to my supervisors, Dr Lee-Anne McKinnell and Lindsay Magnus for the guidance in order to develop an understanding of my project. The encouragement and support of Dr Lee-Anne McKinnell is greatly appreciated.

It is my honor and previledge to thank John Bosco Habarulema for his efforts in proof reading my thesis. I would also like to thank Patrick Sibanda for helping me a lot in programming during data analysis. Cougare Mudzingwa has done the installation of beacon monitor which provided the data used in this project and his effort is greatly acknowledged. I would like to show my gratitude to Mrs Jeanne Cilliers for proof reading my thesis. I would also like to thank all the HMO students and staff for their support and hospitality in any respect during the course of the project.

I would like to send my warm gratitude to my family for the support through out my academic studies. A special thanks goes to my Mum, Dad, brothers and sisters for their continuous love, care and support. I would like to also thank all my friends who have shown support in a number of ways.

Above all, I am most thankful to the Almighty God. He was the major source of strength throughout the project. It is an honor for me to express my deepest gratitude for keeping me under His grace for all this time.

Contents

List of Tables

List of Figures

Chapter 1

Introduction

HF propagation involves transmission and reception of radio signals within a frequency range of 3-30 MHz. HF radio communication depends on the ability of the ionosphere to reflect the signal back to the Earth. Thus for HF communication, surveillance and other propagation purposes, HF propagation prediction models have been developed and validated for some regions, especially in the Northern Hemisphere (e.g Zolesi *et al.*, 2008; McNamara *et al.*, 2007), however, none have concentrated on the African region. Thus computer programs in the form of models to analyze ionospheric parameters and predict HF sky wave system performance over a particular region of interest are required.

1.1 Project Objective

This project aims to validate current HF propagation prediction models over Africa and to develop a good understanding of ionospheric behaviour and its influence on HF propagation. Real-time propagation data is required to validate the models. The Hermanus Magnetic Observatory (HMO) recently became the International Space Environment Service (ISES) Space Weather Regional Warning Centre for Africa and the suite of products offered through this service will include the provision of HF propagation predictions. This project will provide the foundation for the HMO HF propagation prediction service and will be one of the products offered by the HMO Space Weather Centre.

1.2 HF Prediction Models

There are existing prediction programmes for HF propagation signals, but to date none have been fully developed for the African region, and there is a strong need to verify the existing programmes over Africa. HF propagation models such as the Advanced Stand Alone Prediction System (ASAPS) and the Ionospheric Communication Enhanced Profile Analysis & Circuit (ICEPAC) have been developed and are available. ASAPS allows for the prediction of sky wave communication conditions in the HF and lower end of the very high frequency (VHF) radio bands. It is based on an ionospheric model developed by the Ionospheric Prediction Service (IPS), Radio and Space Services of the Australian Department of Industry, Tourism and Resources, and International Telecommunication Union of Radiocommunication (ITU-R)/International Radio Consultative Committee (CCIR) models (http://www.ips.gov.au/Products_and_Services/1/1/2). ASAPS is mostly used by the South African Defence Force as well as the National Intelligence Agency for HF direction finding and therefore ASAPS remains an important tool (Coetzee, 2004).

ICEPAC is a model which predicts the expected performance of the HF communication systems. This model was developed by Environmental Science Services Administration's (ESSA's) Institute for Telecommunication Sciences and Aeronomy (ITSA) (Stewart, 2008). The ICEPAC model is currently used to generate the HF propagation predictions shown on the South African (SA) Space Weather website (http://www.spaceweather.co.za) and was thus used for this project. The prediction accuracy of ICEPAC in the Southern Hemisphere may not necessarily be the same for the Northern Hemisphere where the model was developed. It is known that the model developed included little data for the high latitude and Southern hemisphere regions (Lane, 2005). Therefore, it is important to acquire the most accurate predictions for the Southern hemisphere, and in particular the African region.

1.3 Thesis Overview

The ASAPS and ICEPAC models are of interest in this project since they are the most commonly used models for the prediction of HF propagation conditions in the African region. Therefore, these models need to be validated for the African HF propagation scene using real-time data. The real-time data was obtained from the International Beacon Project (IBP) monitor which is a network system of beacons designed to assist both amateur and commercial HF radio users to assess the current conditions of the ionosphere. The study was performed using two transmitting stations : Ruaraka, Kenya (1.24°S, 36.88°E) and Pretoria, South Africa (25.45°S, 28.10°E), and one receiver station located in Hermanus, South Africa (34.27°S, 19.12°E). The stations were chosen since they are located in the African region of interest. The measured and predicted signal-to-noise ratio (SNR) data will be compared to validate the performance of both ICEPAC and ASAPS. The model which produces a more accurate prediction will be considered for the future improvement of HF propagation prediction over Africa.

This thesis contains six chapters. Chapter 2 gives a brief overview of the theory and background of the ionosphere. A brief description of the two models used in this project is given in Chapter 3. This chapter will present the development of the models and parameters used, as well as the capabilities of these models. Chapter 4 describes the attempts made to validate the HF propagation prediction model. Chapter 5 includes the results obtained and their significance in this field of study. Chapter 6 presents a discussion on the findings and conclusion drawn from the results, as well as possible future work.

Chapter 2

Theoretical Background

2.1 Introduction

This chapter gives the basic theory of HF propagation through the ionosphere. It provides a definition of the ionosphere, as used in this thesis, together with its effects on HF propagation conditions. It also includes a brief description of HF propagation conditions for space weather information.

2.2 Ionosphere

2.2.1 The Sun's effect on the ionosphere

The Sun is the primary source of energy in our solar system and also drives most of the space weather activities. It radiates energy in the form of electromagnetic waves at different wavelengths (Bothmer and Daglis, 2007). The ultraviolet (UV) radiation from the Sun, important for ionisation in the atmosphere, moves towards the Earth's magnetic field. Particle emanating from the Sun interacts with the Earth's magnetic. The Sun's UV radiation affects the ionisation of the upper atmosphere. This section of the atmosphere that is ionised is called the ionosphere. Since the Sun is a continuously evolving star its behaviour and the subsequent effects on the Earth need to be studied.

The so-called sunspot numbers (SSN) are good indicators of the general level of the Sun's effect on the ionosphere (McNamara, 1991). The sunspots appear as

dark spots on the Sun which are counted to give the number known as SSN. The solar cycle shows this behaviour over a long time period. The solar cycle is the main source of periodic variation of solar phenomena driving variations in space weather (McNamara, 1991). The variations in the Sun's radiation cause various physical processes including instabilities in the ionosphere which in turn affect HF propagation (details in section 2.2.3). Therefore, it is important to study the space weather effects of the Sun on the ionosphere and, therefore, on HF propagation.

2.2.2 Regions of the ionosphere

The ionosphere is the upper part of the atmosphere which falls within the mesosphere and thermosphere covering an altitude range from about 60 km to 1000 km. It is a region of ionised gas containing electrically charged particles. Photoionisation is the process in which negatively charged electrons are removed from neutral atoms to leave positively charged ions and free electrons. The schematic diagram shown in figure 2.1 represents the photoionisation process. The free electrons in the ionosphere are important for refraction and reflection of HF radio waves. Photoionisation occurs during the hours in which EUV light from the Sun is shining directly on the atmosphere.

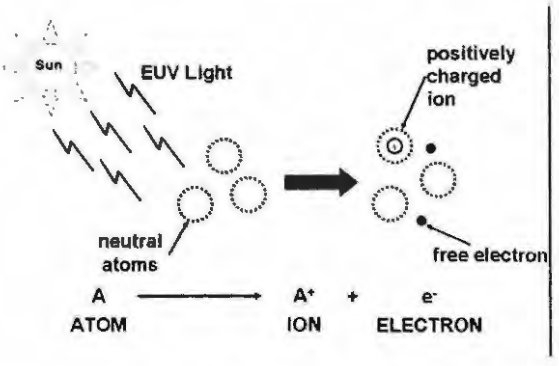

Figure 2.1: A representation of the photoionisation process due to the Sun's extreme ultra violet (EUV) light.

The bottomside ionosphere is that region of the atmosphere between 60 km and about 350 km, and is the region that affects HF (3 - 30 MHz) propagation. This region is divided into four layers : D, E, F1 and F2 layers. These layers are de-

fined by the dominant ions that are present at different altitudes and each layer has a peak electron density associated with it. Electron density is a measure of the ionospheric structure, which is an indicator of the degree of ionisation. The level of ionisation is very important for signal propagation. The higher the level of ionisation, the greater the number of electrons.

The peak electron density of each ionospheric layer is related to the frequency and height of that layer (Gulyaeva, 2009). Thus at greater altitudes, in the F2 layer for example, higher electron densities can be expected and at a lower altitude, E layer, lower electron densities can be expected. The frequency of reflection will depend, among other things, on the electron density of the ionospheric layers. The D region is the lowest in altitude and is important because it has the greatest level of absorption.

The E, F1, sporadic E when present, and F2 layers reflect HF waves. However, the F2 region is the most important region for HF radio propagation as:

- It is present 24 hours of the day.
- Its high altitude allows the longest communication path.
- It usually reflects the highest frequencies in the HF range.

Figure 2.2 shows the location of the ionosphere in the atmosphere and its different layers during day and night times. The lifetime of electrons is greatest in the F2 layer which is one of the reasons why it is present at night. Since the F1 layer is not always present and often merges with the F2 layer, it is not normally considered when examining possible modes of propagation.

The ionisation in the ionosphere varies greatly with the amount of solar radiation present. The processes that cause the ionospheric variation arise from a combination of the rate of change of radiation intensity with time, and the rate of change of the neutral density with time. The altitude at which these rates of change are balanced is where maximum electron density in the ionosphere occurs. Below and above this point the electron density is decreasing. The radiation intensity

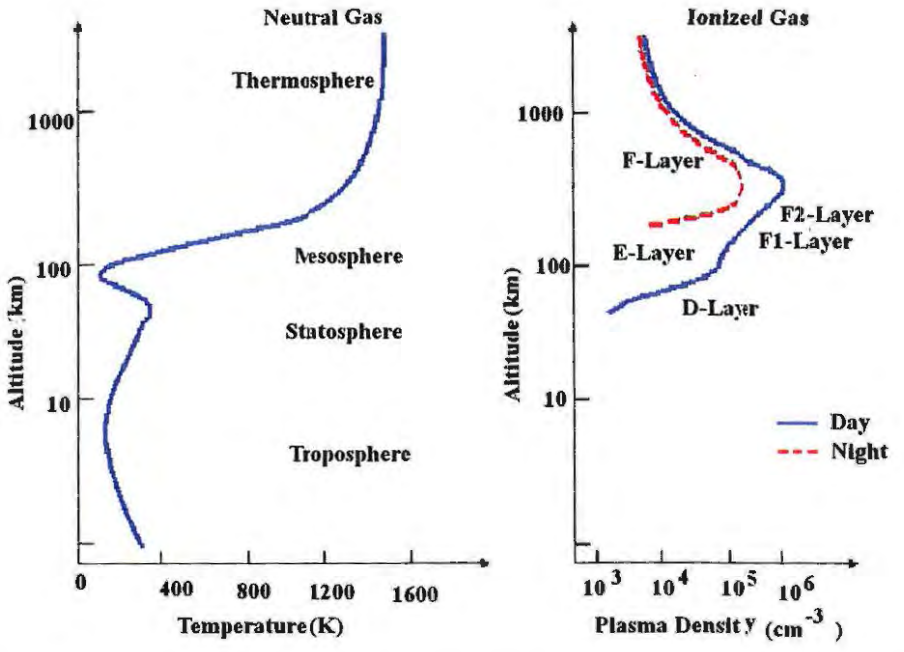

Figure 2.2: The neutral and ionised gas showing the region of the ionosphere during day and night time (Brown, 2009).

looses some energy within the ionosphere leading to low ionisation levels in the lower parts of the ionosphere. Therefore the bottom part of the ionosphere is less ionised and can reflect signals with low frequencies.

Recall that the process of ionisation involves ultraviolet light waves knocking electrons free from their atoms. A reverse process called recombination occurs when the free electrons and positive ions collide with each other. Since these collisions are inevitable, the positive ions return to their original neutral atom state. The recombination process also depends on the time of day. Between the hours of early morning and late afternoon, the rate of ionisation exceeds the rate of recombination. During this period, the ionised layers reach their greatest density and exert maximum influence on radio waves. During the late afternoon and early evening hours, however, the rate of recombination exceeds the rate of ionisation, and the density of the ionised layers begins to decrease. Throughout the night, density continues to decrease, reaching a low point just before sunrise (McNamara, 1991).

2.2.3 Regular variations

There are five main classes of regular variations in the ionosphere: daily, seasonal, latitudinal, 27-day variations and 11-year solar cycle.

Daily variations

Daily variations are a result of the 24-hour rotation of the Earth around its axis. This is due to the dependence of solar zenith angle which contributes to diurnal variations in the ionosphere. When the Sun is overhead (midday) there is high ionisation in the ionosphere and so the foF2 is also at maximum. There is low foF2 during night time than day time.

These variations occur in different layers of the ionosphere. The D layer reflects very low frequency (VLF) waves and is important for long range VLF communications. The reflections of low frequency (LF) and medium frequency (MF) waves for short range communications occur in this layer. It is also capable of absorbing HF waves and has little effect on very high frequency (VHF) waves. The E layer reflects HF waves during the day up to 20 MHz applicable for only oblique propagation, while the F layer is split into two layers, F1 and F2 layers, during the day. The ionisation density of the F1 layer determines the absorption of HF waves passing through to the F2 layer. The F2 layer is the most important layer for long distance HF communication.

Seasonal variations

Seasonal variations moves from one hemisphere to the other with changes in season, due to the relative position of the Sun as the Earth revolving around it,. The seasonal variation of the D, E, and F1 layers corresponds to the highest angle of the Sun, thus the ionisation is greatest during summer. However, for the F2 layer the ionisation is greatest in winter. This leads to the general observation that the operating frequency for F2 layer propagation being higher in winter than in summer (Milan *et al.*, 1997).

Latitudinal variations

The ionosphere differs over the Earth from one place to the other. This is due to variations of the solar zenith angle. The solar zenith angle is the angle between the local zenith and the line of sight to the Sun. It describes the position of the Sun with respect to the zenith. The ionosphere has considerable variation with latitude (McNamara, 1991).

27-day sunspot cycle

Due to the 27-day rotation of the sun around its own axis, the appearance and disappearance of the sunspots are visible at 27-day intervals. This cycle causes variations in the ionisation density of the layers on a daily basis. The greatest fluctuations occur in the F2 layer. For this reason, precise predictions of the frequency are not possible and these fluctuations must be considered when calculating frequencies for long-distance communication.

11-year solar cycle

The phenomenon of the appearance and disappearance of dark spots on the surface of the Sun is called sunspots. They are caused by violent eruptions on the Sun and are characterised by unexpected strong magnetic fields. They are responsible for severe space weather events and subsequent ionospheric disturbances. The regular cycles of sunspot activity have both minimum and maximum levels that occur approximately every 11 years. During maximum (or high) sunspot activity, the ionisation density of all layers increases and higher operating frequencies must be used for long-distance communication.

2.2.4 Irregular variations

Irregular variations in ionospheric conditions also have an important effect on radio wave propagation. These variations are unpredictable and can affect communication capabilities without any warning. The common irregular variations are sporadic-E, spread of the ionospheric F layer, sudden ionospheric disturbances and ionospheric storms.

Sporadic E

Sporadic E is an unpredictable natural phenomenon that occurs in the E layer of the ionosphere. This natural phenomenon may form at any time during the day or night (http://www.amfmdx.net/fmdx/sporadic-e.html). Sometimes sporadic E is so thin that radiation waves penetrate it easily and sometimes it is heavily ionised. The sporadic E layer could have a very high frequency and can be greater than twice the normal frequency of the ionosphere. This condition makes long-distance transmission of signals at higher frequencies possible.

Sudden ionospheric disturbances (SIDs)

SIDs are extremely unusual irregularities within the ionosphere. When SIDs occur, long-distance propagation of HF radio waves is usually "blanked out". The solar eruption produces an unusually intense burst of UV light, which is not absorbed by the F2, F1, and E layers, but rather causes a sudden abnormal increase in the ionisation density of the D layer. Therefore, frequencies above 1 or 2 MHz are unable to penetrate the D layer (Goodman, 2005).

Ionospheric storms

Ionospheric storms are associated with disturbances in the Earth's magnetic field. Ionospheric storms result from particle radiation from the Sun and these particles have a slower velocity than UV light waves. The ionospheric storms that are associated with sunspot activity may occur anytime from two days before an active sunspot crosses until four days after it passes the central meridian. During ionospheric storms, the behaviour of the ionosphere is mainly characterized by a decrease or an increase in electron density known as the negative and positive ionospheric storms (Prölss, 2004). Critical frequencies are lower than normal especially for the F2 layer. Ionospheric storms affect the higher F2 layer first, reducing its ion density. Lower layers are less affected by the storms unless the disturbances are great. The range of frequencies that can be used for communication is much smaller than normal and communication is possible only at lower working frequencies (McNamara, 1991).

2.3 High Frequency (HF) Propagation

Radio signals can travel over vast distances. On shortwave HF bands, signals can be heard regularly from the other side of the globe. HF propagation has long been of interest. It was used back in the earliest days of wireless to provide worldwide communication, and even today HF propagation is still used by many organisations from international broadcast stations and radio amateurs through to shipping services, weather stations and a variety of other two-way radio communication systems and mobile radio communication systems.

The way in which radio signals propagate is of prime importance to anyone associated with radio communication. Signal propagation through the ionosphere in the HF bands (3-30 MHz) enables stations to have worldwide coverage using relatively little power and relatively low-cost equipment. Other important uses of the ionosphere for radio propagation are adequate bandwidths for audio communication and adequate signal strength over long distances. The disadvantages of using the ionosphere for radio propagation includes variability of propagation conditions, frequent frequency changes, time dispersion due to interference of waves from multiple paths, large and rapid amplitude and phase fluctuations and also the interruption by ionospheric storms (McNamara, 1991).

2.3.1 Ray-tracing through the ionosphere

An application of the use of the ionosphere for HF radio propagation is the process of performing Single Site Location (SSL) using the technique of ray-tracing. Figure 2.3 shows the ray-tracing of a signal through the ionosphere to a receiver. The distance between a transmitter and a receiver is known as the ground range. The take-off angle and the height at which the signal is reflected is also illustrated. The technique of ray-tracing takes advantage of the fact that radio waves transmitted from one part of the Earth will be reflected within the ionosphere and returned to Earth at another location (Haselgrove, 1954). To determine the ground range

between the receiver and the transmitter, a good knowledge of ionospheric behaviour, as well as the radio frequency and elevation angle of the incoming signal, is required.

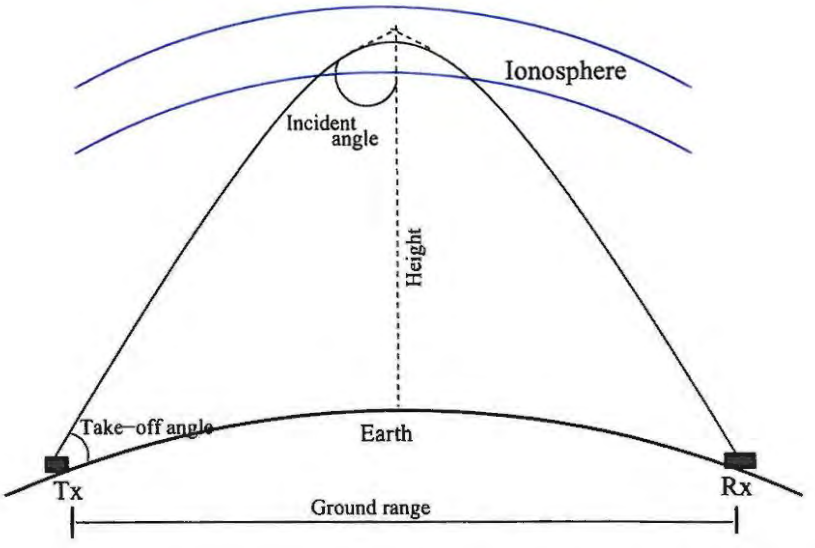

Figure 2.3: Ray-tracing of a signal through the ionosphere.

According to secent law :

$$MUF = f_c \times sec(\phi)$$

where MUF is the maximum usable frequency, f_c the frequency of the ionosphere and ϕ is the angle of incidence of the ray at the base of the ionosphere. Therefore, knowing the frequency and the MUF, the incidence angle of the incoming signal can be determined (McNamara, 1991). There are different ways in which a radio signal can travel from a transmitter to a receiver such as via ground wave or skywave propagation. This thesis will deal with HF propagation via sky wave propagation.

2.3.2 Skywave propagation

Skywave propagation happens when a HF radio signal is reflected by the ionosphere to a receiver. This is distinct from "ground wave" propagation, which is direct propagation from transmitter to receiver. Most long-distance HF radio communication is a result of skywave propagation. The distance traveled by a signal from a transmitter before reaching the Earth again is called the skip distance. The area between the limit of the ground wave coverage and where the skywave returns to Earth and where no signal can be received, is called the dead zone or the skip zone.

Sometimes a transmitted wave propagates through the E, F1 and F2 layers for certain frequencies. Different ionospheric layers reflect varying frequency ranges. All these layers have frequencies, foE, foF1 and foF2, below which transmitted frequencies are reflected by the E, F1 and F2 layers respectively. Above these frequencies, the transmitted signals propagate through the respective layers and end up in outerspace when the frequency is greater than foF2.

There are upper and lower frequency bounds for communication which are called the MUF and Lowest Usable Frequency (LUF). The MUF is the highest frequency that can be reflected back to the Earth from the ionosphere. It is reflected below the maximum electron density within a given layer in the ionosphere. If the frequency is higher than the MUF, the signal will pass through the ionosphere as mentioned above, and if the frequency is lower than the LUF, then the signal will be absorbed in the D region.

2.3.3 Multiple hops

Very often signals will be heard over distances which are larger than would be possible with just one reflection. For example, it is quite common to hear stations from the other side of the globe and this is considerably in excess of the maximum skip distance even for the F2 layer. The most common way for signals to travel over greater distances is by multiple reflections (Sizun, 2004). It is found that when a signal is reflected back to Earth by the ionosphere then the Earth can reflect it back up to the ionosphere. In this way signals can travel to anywhere on

the globe.

2.3.4 Propagation modes

A skywave may propagate from a transmitter to a receiver through the E layer by means of one or more reflections. The mode reflected by a particular layer, e.g. E layer, which requires the least number of hops from a transmitter to a receiver is called the first order mode of E layer. The mode that requires one extra hop is called the second order mode. Figure 2.4 shows the simple propagation modes of the E and F layers with first and 2nd order modes.

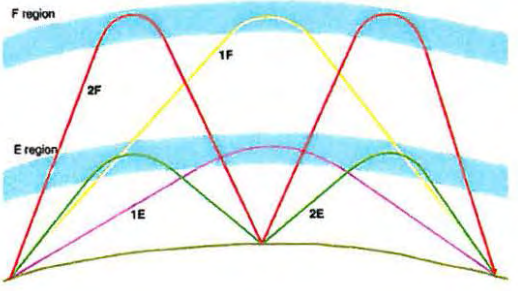

Figure 2.4: An example of the simple propagation modes of the E and F layers.

2.3.5 Frequency, path length and elevation angle

The most important variables in the HF propagation path are the frequency of transmission, the path length between a transmitter and a receiver and the antenna elevation angle.

Figure 2.5 shows the possible changes to the ray paths when each of these variables is fixed in turn. For a fixed elevation angle, the path length is different for different frequencies. A short path length is available for low frequencies and as the frequency increases the path length also increases, as shown by signal 3 in figure 2.5(a). If the frequency is higher than the MUF, then the signal will pass through the ionosphere, as shown by signal 4 in figure 2.5(a).

If the path length is fixed then both the frequency to be used and the elevation angle will be adjusted for the signal to arrive at the same receiver location, as shown

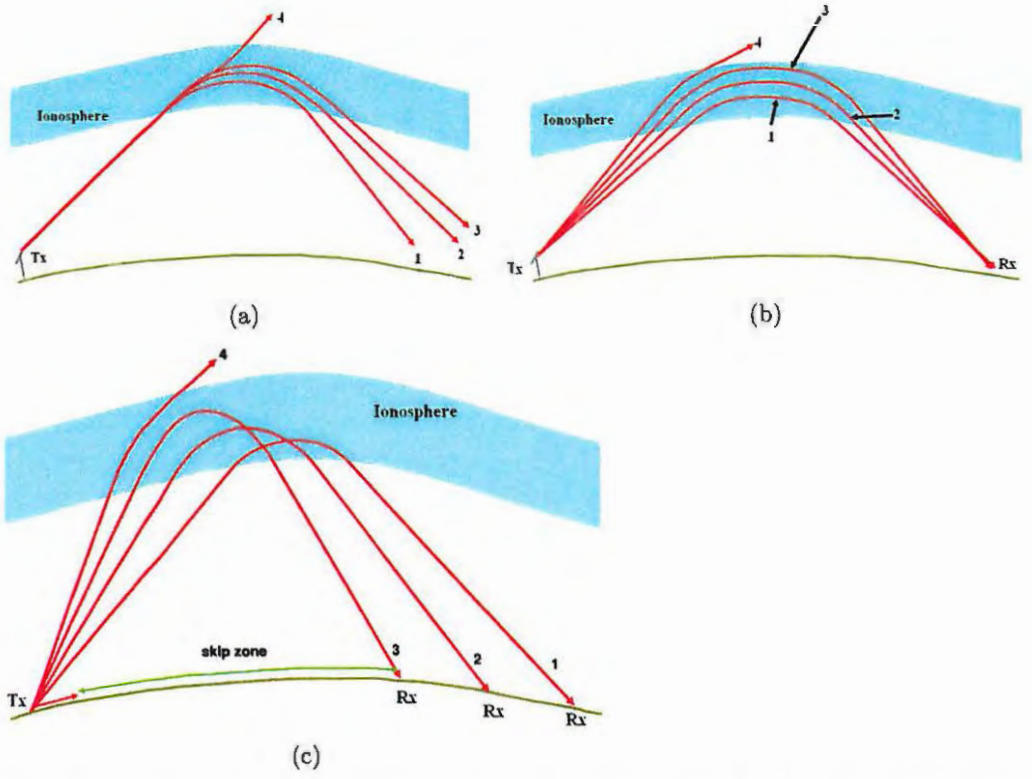

Figure 2.5: An example of the relation between elevation angle, path length and frequency : (a) the fixed elevation angle, (b) the fixed path length and (c) the fixed frequency.

in figure 2.5(b). For a fixed frequency the path length decreases as the elevation angle increases, as the signal is reflected from a higher level of the ionosphere. If the elevation angle increases beyond the elevation angle then the signal will pass through the ionosphere and will not be received, as shown by signal 4 in figure 2.5(c).

2.4 Space Weather Effects on HF propagation

Space weather describes the conditions in space that affect Earth and human technological systems. Space weather is a consequence of the behaviour of the Sun, the nature of Earth's magnetic field and atmosphere, and our location in the solar system. HF communication is affected by the ionospheric disturbances caused by the solar-produced interactions with the Earth's space environment. Adverse space

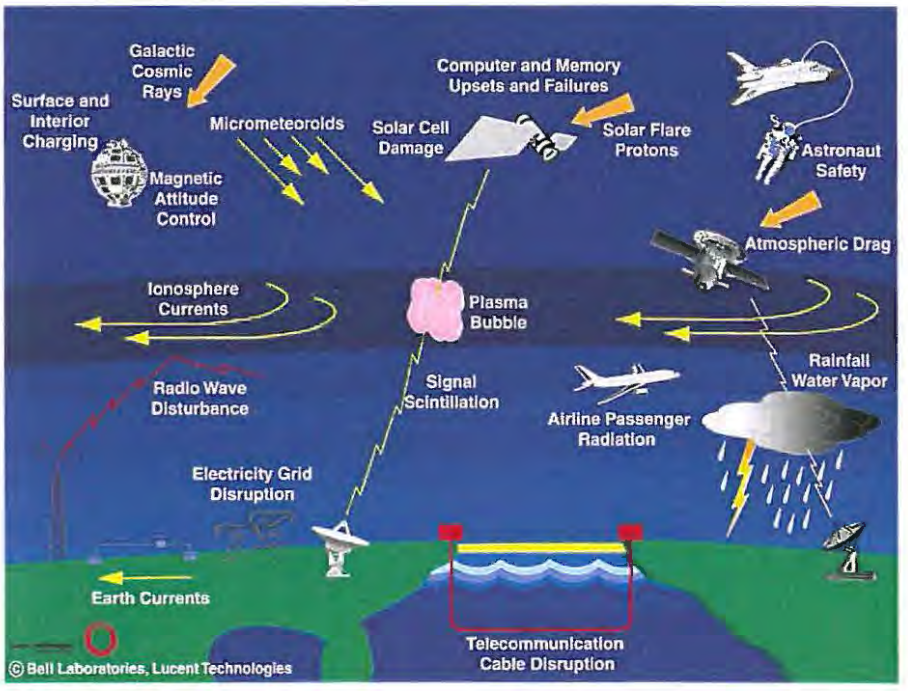

Figure 2.6: The identified space weather effects on technological systems. Figure obtained from http://www.space.noa.gr/daglis/activities/asi2000.html.

weather is one of the principal threats to modern technology. International space science programmes study solar activity, the propagation of energy from the Sun through the interplanetary medium, the energy coupling in the magnetosphere, and the redistribution in the middle and upper atmospheres (Daglis, 2004). With the increase in technological systems the need for accurate space weather predictions and forecasts has increased (shown in figure 2.6). This has meant that there is an increased demand for HF propagation prediction conditions, particularly in the defence and navigation industries, and the ability to accurately predict space weather conditions will become more important in the future as solar cycle 24 progresses.

2.5 Summary

Studying ionospheric behaviour is very important for HF propagation and other radio wave applications since the ionosphere is the main source of HF radio wave

reflection. The variability of the ionosphere makes HF communication unstable, and therefore models to predict signal propagation for different ionospheric conditions are crucial. The HF propagation models used in this project will be described in Chapter 3. The models to be evaluated in this project are those currently being applied in South Africa for HF propagation prediction.

Chapter 3

Current HF Propagation Models

3.1 Introduction

This chapter provides a description of the current HF propagation models considered in this project. The HF propagation models which are considered in this project are the Ionospheric Communications Enhanced Profile Analysis and Circuit (ICEPAC) and Advanced Stand Alone Prediction System (ASAPS) models. These models were chosen since they are the most commonly used HF propagation models in South Africa and other African regions. ICEPAC is used at the Space Weather South African (SWSA) to predict HF propagation conditions and ASAPS is used by the South African Defence Force and National Intelligence for HF direction finding (Coetzee, 2004).

3.2 Introduction to ICEPAC Model

For many years a number of organizations have been using the HF spectrum to communicate over long distances. In the late 1930's it was recognized that these communication systems exhibit some variations in performance. It was demonstrated by research that these variations in HF system performance were related to the changes in the ionosphere. The Ionospheric Communications Analysis and Prediction programme (IONCAP) was developed by the Institute for Telecommunication Sciences (ITS) and its predecessor organizations, with the primary aim being to investigate ionospheric parameters and determine their effect on radio waves and the associated reliability of HF circuits (Stewart, 2008).

A major problem with IONCAP was its poor performance in the polar regions and, therefore, some of the older electron density profile structures were used. This problem was corrected by transforming IONCAP into ICEPAC by adding the Ionospheric Conductivity and Electron Density (ICED) profile model (Tascione *et al.*, 1988). The ICED profile model is a statistical model of the large-scale features of the Northern Hemisphere. The model recognizes the different physical processes that exist in the different regions of the ionosphere. It contains distinct algorithms for the sub-auroral trough, auroral zone, and polar cap (Stewart, 2008).

3.3 ICEPAC Model

The ICEPAC prediction programme is one of the modelling tools which is used for predicting HF propagation over the African region. This programme predicts the expected performance of HF broadcast systems. It is useful in the planning and operation of HF transmissions for the four seasons, different sunspot activities, hours of the day, and geographical locations. The programme is divided into seven independent sections (Stewart, 2008):

1. input subroutines,
2. path geometry subroutines,
3. antenna subroutines,
4. ionospheric parameter subroutines,
5. maximum usable frequency subroutines,
6. system performance subroutines, and
7. output subroutines.

This prediction programme can be implemented in different ways e.g.

- ICEPAC - a point-to-point mode, meaning that the propagation for a path between a transmitter and a receiver is calculated.

- ICEAREA - this produces area coverage predictions.
- S/I ICEPAC - calculates signal-to-interference in point-to-point mode (Stewart, 2008).

3.3.1 Input parameters of ICEPAC

The ICEPAC prediction model requires setting a number of parameters used in the model. This section provides details on these parameters and how they may affect predictions if not properly set. For the purpose of the study ICEPAC point-to-point prediction was chosen. Figure 3.1 shows the ICEPAC point-to-point prediction window with different input parameters.

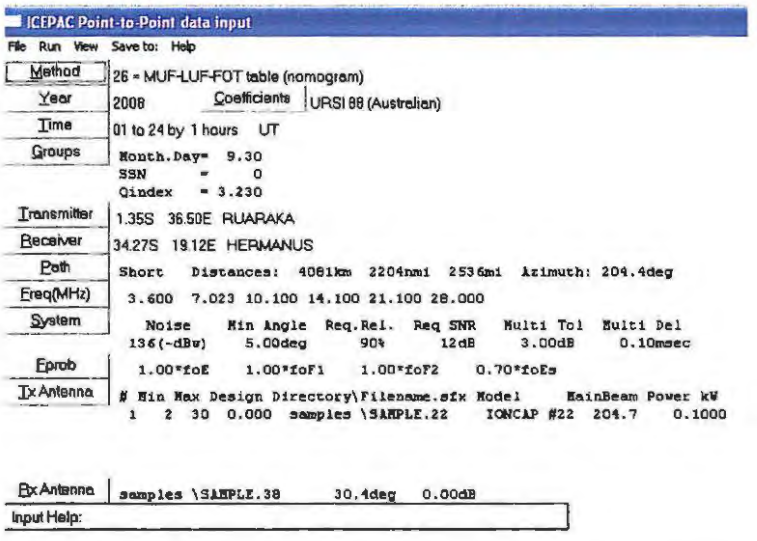

Figure 3.1: A point-to-point analysis tool showing the main menu and settings.

- **Method**

Method is the parameter which controls the type of programme analysis and prediction performed. Many of these methods differ only in the presentation of the output. There are 30 different methods to choose from when predicting HF propagation conditions. Most of the work done for this project used a default "Method 20", which is a complete system performance and "Method 26" which is a MUF-LUF-FOT (Frequency of Optimum Transmission) table prediction. The reason

for using "Method 20" is that it is the recommended way of modelling full system performance on HF paths (Lane, 2005). Also, the predictions of "Method 20" and "Method 26" have some of the output parameters such as signal-to-noise ratio (SNR), take-off angle, MUF, LUF and FOT which are presented in graphic form on the SA space weather website.

- **Coefficients**

There are two options under the parameter "coefficients", namely the URSI 88 (Australian) and CCIR (Oslo) coefficients. These are the ionospheric parameters which are derived by fitting equations into the measured data in the form of numerical coefficients based on a particular computation method (Sheikh, 1979). Two organizations, International Union of Radio Science (URSI) and International Radio Consultative Committee (CCIR) are of particular importance in the collection and evaluation of ionospheric data for communication purposes. URSI deals with the scientific aspects of radio wave propagation and coordinates ionospheric observations on an international basis. CCIR has the International Telecommunication Union (ITU) and promotes international standardization of models for the propagation medium and radio noise environment (Thrane *et al.*, 1994).

URSI 88 (Australian) coefficients are a linear fit between a low (1975 - 1976) and high SSN (1978 - 1979). They were developed in Australia and accepted by URSI in 1988. In contrast to CCIR, the URSI coefficients also contain data for the ocean areas. The measurements in the CCIR database are obtained from ionosondes worldwide for 1954 to 1958 and 1964. The URSI 88 and CCIR coefficients are stored in the ICEPAC database in a binary format. These are the parameters which contain the structure of the ionosphere and, since they are hard wired into the code, it is not possible to change the ionospheric configuration to suit a different location.

- **Groups**

There are input parameters within the "Group" which are: the dates ("Month.Day"), sunspot numbers (SSN) and Q_{index} as seen in figure 3.2. The "Month.Day" gives an option to select the month and the day for which the predictions are performed. To generate the monthly predictions, only the month is set and "00" is used for

Q_e	K_p	A_p	Geomagnetic Activity
0.0	0.0 for values of $Q_e < 3$; $K_p = Q_e/3$	0	Quiet
1.0	0.33		Quiet
2.0	0.67		Quiet
3.0	1.0 for values of $Q_e > 3$; $K_p = Q_e$-2	3	Quiet
4.0	2.0	7	Unsettled
5.0	3.0	15	Active
6.0	4.0	27	Minor storms
7.0	5.0	48	Major storms
8.0	6.0	60	Major storms

Table 3.1: The current relationship between Q_e and K_p, if K_p is known (De Canck, 2006b).

day, thus "9.00" for September predictions. The SSN is the indication of solar activity and Q_{index} or Q_e is the effective geomagnetic activity index. This index can be obtained if the planetary magnetic field index (K_p) is known. These are the main factors to consider when determining the propagation path. Table 3.1 shows the relationship between Q_e and K_p during quiet and storm conditions.

Besides the SSN, day of the month and the Q_{index}, there is also effective SSN. The effective SSN can be used as an alternative to SSN. This index can be calculated from the measured ionospheric foF2 (critical frequency of the F2 layer) values for the exact time and location (De Canck, 2006b). The ionospheric parameter, foF2, is the maximum frequency below which the vertical transmitted wave is reflected back to Earth. It is directly related to the maximum ionospheric electron density by :

$$N/m^{-3} = 1.24 \times 10^{10}(f/MHz)^2 \tag{3.1}$$

which is important in ionospheric modelling (McKinnell, 2002).

Figure 3.2 shows how to calculate the effective SSN after input of the foF2 values. If more than one foF2 value is available, then the average effective SSN is used. If effective SSN is used, ICEPAC assumes that there is vertical ionosonde information available for one or more locations. The ideal sounder location would be the midpoint of the path of interest. The further away from this location, the less

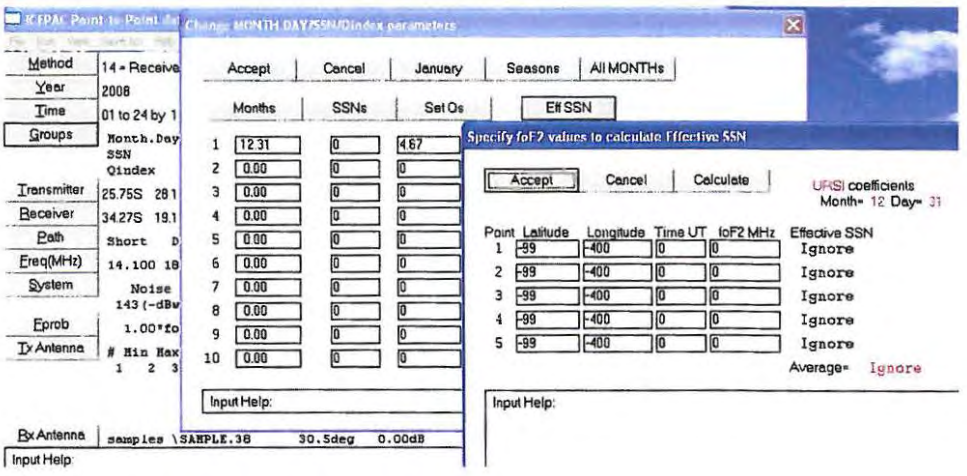

Figure 3.2: An input screen showing where to specify foF2 values to calculate effective SSN.

confidence can be placed in the results.

- **Transmitter and Receiver Location**

The transmitter and the receiver contain the geographical coordinates (longitude and latitude) and the name of the transmitter or receiver location. This will provide the path of interest for HF communications. For example, figure 3.1 shows that the signal for this example is transmitted from Ruaraka, Kenya (1.24°S, 36.88°E) and received in Hermanus, South Africa (34.27°S, 19.12°E).

- **Path and Frequency**

The signal path is important when attempting to receive signals from a particular area. The signal can either propagate through the short or the long path, depending on target location, time of the day, and the antenna gain. Long path means longer than 10 000 km and in this case "method 21" is used. The frequency ranges between 2-30 MHz on the prediction graph generated as output by the ICEPAC model. Therefore the frequencies are set within this range, e.g., for the Amateur Radio bands, 3.06, 7.01, 14.1 MHz etc., would be used.

- **Systems**

The prediction system has six different fields and is one of the most important settings in ICEPAC because it affects the prediction accuracy and reliability.

Man-made Noise level at 3MHz

Man-made noise may arise from a number of sources such as power lines, industrial machinery, ignition systems, etc. A value representing the man-made noise is inserted according to the type of location. These values are as follows:
a. -125 dBW for industrial area.
b. -136 dBW for residential area.
c. -148 dBW for rural area.
d. -164 dBW for remote unpopulous (Stewart, 2008).

In choosing a value to represent the man-made noise, the location of the receiver must be considered. For example, if the signal is transmitted from an industrial area to be received in a rural area, the value -148 dBW is considered to be representative of the man-made noise. Therefore, it is important to know the type of location from which the receiver will be operating.

Minimum take-off angle

The take-off angle affects the signal strength at the target location. If the take-off angle is small then the radio signal travels a longer distance than when the take-off angle is large. In communicating to a point which is at a distance of about 1000 km away using a 20 meter band (14.2 MHz) radio signal, it would be a good choice to use as small a take-off angle as possible.

Required circuit reliability

The term "reliability" means "time availability". If the required reliability is set to 50%, then the resulting predictions will be most accurate during 15 days over a 30-day month and a 90% prediction accuracy can be expected for 27 days. The amateur working conditions match with a 90% reliability. It would be interesting to set this parameter to 50% and 90% to see the change in the signal strength and power at the target location. In the experimental trials the reliability reached

Mode	Required SNR in 1Hz bandwidth
AM	51 dB
SSB	48 dB
CW	31 dB

Table 3.2: Various modes of the recommended required SNR (Luetzelschwab, 2004).

90% when the geomagnetic index $A_p \leq 27$ and K_p index ≤ 4 (i.e. quiet time conditions).

Required signal-to-noise ratio (SNR)

The required SNR ranges between -30 and 99 dB.Hz which is a very wide power spectrum. The SNR is the ratio of the hourly **median signal power** in a specified bandwidth relative to the hourly **median noise** in a 1 Hertz bandwidth, a relationship that can be described by the following:

$$\text{SNR (dB)} = 10 + 10\log(\lambda),$$
$$\text{where } \lambda = \text{bandwidth in Hz}$$

The SNR is necessary to achieve the type and quality of service required. The recommended required SNR for various modes is shown in table 3.2 where AM stands for amplitude modulation, SSB stands for single sideband and CW mode stands for continuous wave. CW mode was selected for the predictions used in this study since the real-time measurements are recorded in the CW mode. Details about these modes are given by Dennison and Fielding (2007).

Multipath Power Tolerance (dB)

Multipath power tolerance indicates the maximum difference in delayed signal power between skywave modes that permits satisfactory system performance in the presence of multiple signals. The multipath probability estimates whether or not multiple skywave modes will exist between a specified power tolerance and outside the time delay tolerance. The use of various modes on multiple skywave paths have effects on the signal strength. Multipath power tolerance ranges between 0 and 40 dB. This parameter only affects the output parameter MPROB (probability of additional mode in multipath tolerances) and so the SNR graph remains unchanged.

Maximum tolerance time delay

This is also called the multipath delay and is measured in milliseconds. This is the maximum difference in delay time and can also affect the MPROB parameter. A very large time delay produces a perceptible decrease in the signal strength.

- **Transmitter (Tx) and receiver (Rx) antennas**

The antenna system is part of the electrical circuit of a transmitter (Tx) and receiver (Rx). The Tx antenna radiates the signal power from the transmitter to the receiver location. There are factors to consider when selecting an antenna and section 3.3 will provide a description of these factors. ICEPAC has the antenna files available in the "ITS HF Propagation" database which contains the parameters designed for a particular antenna system. These files contain the antenna name and other parameters like conductivity, which will be described in the next section. The Tx and Rx antenna parameters are the last parameters to be set as shown in figure 3.1.

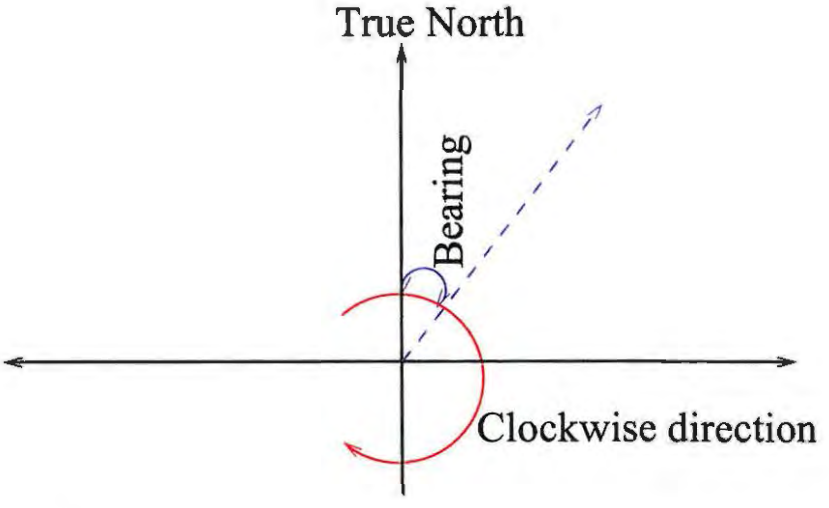

Figure 3.3: The antenna bearing measured from true north in a clockwise direction.

In ICEPAC the Tx antenna has the option of setting the direction of the main beam (in degrees) and the transmitter power (in kilowatts). The Rx antenna has

the option of setting the bearing angle (in degrees) and the gain (in dBi), which is the measure of the radiation intensity for a given direction with respect to isotropic radiation intensity. A bearing is the direction of an object from the observer. In ICEPAC the Rx bearing is the angle measured from true north of the Rx terminal with the angle increasing in a clockwise direction, shown in figure 3.3. Therefore, to receive a good signal, a Rx bearing should point in the direction of the Tx main beam. If the Rx bearing is pointing in a different direction, then a weak signal may be received.

3.3.2 Output parameters of ICEPAC

After setting all the parameters, the option **"Run"** can be selected to process the predictions. This option allows for the following parameters to be adjusted in relation to the outputs of interest: "Circuit", "Graph", "Batch", "Distance", "Time", and one of them can be chosen, depending on the type of predictions to be computed. The data is obtained by clicking on the **"Run"** $\longrightarrow$ **"Circuit"** button. The data output depends on the input method used. The results using two different methods are shown below. Figures 3.4 and 3.5 show point-to-point prediction outputs using methods 20 and 26. The definitions of some of the parameters for method 20 output are:

FREQ - Frequency of transmission in MHz,
MODE - Propagation mode,
ANGLE - Radiation angle in degrees,
DELAY - Time delay in milliseconds,
V HITE - Virtual height in km,
MUFday - Expected percentage of the days in a month for skywave propagation at MUF,
LOSS - Median system loss in dB,
SNR - Median signal-to-noise ratio in dB,
REL - Time availability, % time which SNR exceeds the required SNR,
TGAIN - Transmitter antenna gain in dB,
RGAIN - Receiver antenna gain in dB,

For method 26 the definitions of the parameters commonly used are :

```
    URSI Coeff(Daily)          METHOD 20   ICEPAC  Version 050119W PAGE   1

MAR,31 2009 (Daily)  SSN =   0.     Qeff= 3.1      Minimum Angle  3.00 deg
PRETORIA            Hermanus                AZIMUTHS          N. MI.      KM
25.75 S   28.17 E - 34.27 S   19.12 E    220.42   44.97     694.3   1285.8
XMTR  2-30 IONCAP #22[samples\SAMPLE.22    ] Az=204.8 OFFaz= 15.6   0.100kW
RCVR  2-30 HFMUFES#38[samples\SAMPLE.38    ] Az= 30.5 OFFaz= 14.5
3 MHZ NOISE = -143.0 DBW     REQ. REL = .90    REQ. SNR = 31.0 DB
MULTIPATH POWER TOLERANCE =  3.0 DB   MULTIPATH DELAY TOLERANCE =  0.100 MS

 1.0  4.9  1.8  2.8  3.0  4.2  5.8  6.8  0.0  0.0  0.0  0.0  0.0 FREQ
      1F2  1F2  1F2  1F2  1F2  1F2  1F2    -    -    -    -    - MODE
     26.5 18.3 18.6 18.7 20.8 26.5 26.5    -    -    -    -    - ANGLE
      5.1  4.7  4.7  4.7  4.8  5.1  5.1    -    -    -    -    - DELAY
      372  254  258  260  288  372  372    -    -    -    -    - V HITE
     0.50 1.00 1.00 0.99 0.82 0.19 0.03    -    -    -    -    - MUFday
      127  128  128  127  124  135  151    -    -    -    -    - LOSS
       13    8   14   14   17    5  -10    -    -    -    -    - DBU
     -107 -104 -107 -106 -104 -115 -131    -    -    -    -    - S DBW
     -148 -135 -143 -143 -146 -150 -152    -    -    -    -    - N DBW
       41   31   36   37   42   35   20    -    -    -    -    - SNR
        5    9    4    3   -1   15   35    -    -    -    -    - RPWRG
     0.81 0.51 0.77 0.81 0.91 0.60 0.28    -    -    -    -    - REL
     0.00 0.25 0.00 0.00 0.00 0.00 0.00    -    -    -    -    - MPROB
     0.42 0.23 0.38 0.40 0.51 0.28 0.14    -    -    -    -    - S PRB
     10.9  0.2  1.2  1.3  4.5 16.8 22.2    -    -    -    -    - SIG LW
      9.8  8.8  4.8  4.9  4.8 15.4 23.2    -    -    -    -    - SIG UP
     14.2  9.1  9.1  9.1 10.1 19.1 24.1    -    -    -    -    - SNR LW
     11.1 10.9  7.7  7.7  7.3 16.3 23.8    -    -    -    -    - SNR UP
     -2.7  0.0 -2.9 -3.0 -3.1 -2.8 -2.8    -    -    -    -    - TGAIN
      1.1  0.0 -4.6 -3.8 -1.2  2.2  2.2    -    -    -    -    - RGAIN
       26   22   27   28   32   16   -4    -    -    -    -    - SNRxx
      -77  -74  -77  -76  -74  -85 -101    -    -    -    -    - DBM
```

Figure 3.4: The output parameters of "Method 20" represented for complete system performance prediction.

FOT - Frequency of optimum transmission/ possible working frequency.

HPF - Highest possible frequency.

MUF - Maximum usable frequency.

LUF - Lowest usable frequency.

The prediction output can also be represented graphically, as shown in figures 3.6 and 3.7 for SNR and frequency predictions respectively. Figure 3.6 shows the contour plot of SNR, one of the output parameters, with frequency and time of the day. This illustrates the signal strength for different frequencies at a particular hour, for example, when transmitting a 14 MHz signal at 8:00 UT, the SNR would be between 30 and 35 dB. Figure 3.7 represents the possible frequencies to be used at any time of the day. It shows the maximum and the minimum frequencies, but

```
I    URSI Coeff(Daily)          METHOD 26   ICEPAC  Version 050119W PAGE   1

 SEP,23 2008 (Daily)  SSN =   9.     Qeff= 3.0      Minimum Angle  3.00 deg
 Ruaraka              Hermanus                AZIMUTHS          N. MI.      KM
  1.24 S   36.88 E - 34.27 S   19.12 E    284.78   30.47     2219.2    4109.6
 XMTR  2-30 IONCAP 822[samples\SAMPLE.22     ] Az=284.8 OFFaz=360.0    0.100kW
 RCVR  2-30 HFMUFES830[samples\SAMPLE.30     ] Az= 30.5 OFFaz=360.0
 3 MHZ NOISE = -143.0 DBW     REQ. REL = .90    REQ. SNR = 31.0 DB

    UT    LT    FOT    HPF  ESMUF    MUF    LUF

   1.0   3.5   4.39   7.72   3.61   5.85  -5.85
   2.0   4.5   4.37   7.69   3.61   5.83  -5.83
   3.0   5.5   6.10  10.73   4.82   8.13  -7.82
   4.0   6.5  10.44  14.59   4.92  12.58  -8.99
   5.0   7.5  13.97  19.53   6.27  16.83 -16.83
   6.0   8.5  15.85  22.15   7.84  19.09 -19.09
   7.0   9.5  15.47  21.62   9.38  18.64 -19.44
   8.0  10.5  15.32  21.56  10.64  18.92 -18.92
   9.0  11.5  15.62  21.98  11.47  19.28 -19.28
  10.0  12.5  16.09  22.19  11.82  19.47 -19.47
  11.0  13.5  15.95  22.44  11.78  19.69 -19.14
  12.0  14.5  16.53  23.49  11.12  19.91 -19.00
  13.0  15.5  16.66  23.69  10.14  20.07 -19.25
  14.0  16.5  16.32  23.20   8.99  19.67 -18.90
  15.0  17.5  15.94  22.66   7.57  19.21 -18.48
  16.0  18.5  12.48  23.91   6.13  17.98 -19.67
  17.0  19.5  10.95  21.11   4.87  15.87 -16.86
  18.0  20.5   9.32  17.96   3.99  13.58 -13.58
  19.0  21.5   8.00  15.43   3.57  11.60  -7.97
  20.0  22.5   7.02  13.28   3.54  10.16 -10.15
  21.0  23.5   6.96  11.75   3.73   9.03  -9.03
  22.0   0.5   6.34  10.71   3.92   8.24  -8.24
  23.0   1.5   5.98  10.09   3.95   7.76  -7.76
  24.0   2.5   5.22   9.19   3.80   6.96  -6.96
```

Figure 3.5: The output parameters of "Method 26" for computing MUF-LUF-FOT table.

a good choice would be the frequency of optimum transmission.

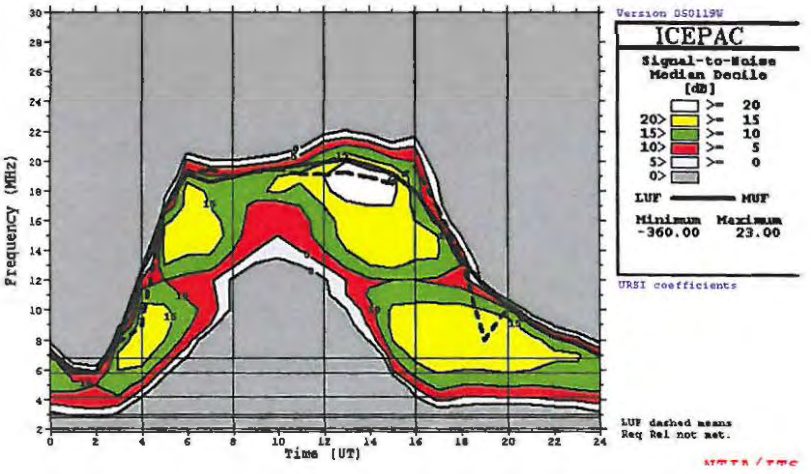

Figure 3.6: The field strength prediction graph showing the contour of SNR.

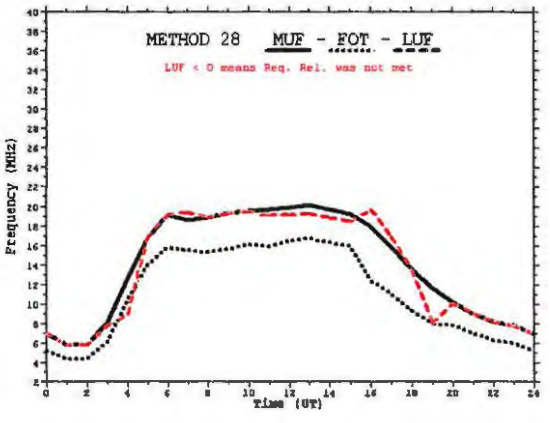

Figure 3.7: The MUF-FOT-LUF graph representing the frequency boundaries.

3.4 ASAPS Model

3.4.1 Introduction

ASAPS allows for the prediction of skywave communication conditions in the HF (High Frequency) and low VHF (Very High Frequency) radio spectrum or Short Wave Band (1 to 45 MHz). This model provides two types of predictions : field strength (point-to-point) and area predictions. The field strength predictions provide information about the SNR, take-off angle, best usable frequency (BUF), Noise, etc. The area prediction gives an area coverage of a certain parameter, for example, frequency which can be transmitted within that area. The ASAPS model has different versions and this section of the project only describes version 5.1 (V5.1) of this model.

3.4.2 Brief description of ASAPS

For over 50 years radio communicators have been assisted by IPS Radio and Space Services of the Australian Department of Industry, Science and Resources (ISR) to optimise the probability of successfully transmitting radio waves/messages via the ionosphere. Now the focus of IPS has shifted from long-term planning to real-time forecasting. Software tools such as ASAPS have been developed to make it easier for frequency managers to produce frequency lists for the various major communication tasks, such as routine HF communications, direction finding, large area surveillance, and measures for protecting the secure transfer of messages. ASAPS was developed to access data from a real-time ionospheric model (RTIM) via the IPS webpages. The RTIM was generated using the data from the Ionospheric Prediction Service Network (IPSNET) of ionospheric stations and many overseas stations (Caruana, 2009).

3.4.3 Input parameters

Most of the input parameters of ASAPS are more or less similar to the ones used in ICEPAC models. But the ASAPS V5.1 model does not contain the "coefficients" parameter as in the ICEPAC model. ICEPAC uses SSN and Q_e whereas ASAPS uses the T-index which means that ICEPAC uses two indices and ASAPS one

index at a time for computing HF propagation predictions. The T-index which is the representation of effective sunspot number, is developed by IPS and is based on the ionospheric foF2 measurements obtained from ionograms.

Even though the T-index is the one mostly used in ASAPS, two other indices are also used, i.e. SSN and the 10.7 cm solar flux. Therefore, instead of using the T-index, one of these indices may be used. The SSN data used in this work was obtained from the Space Physics Interactive Data Resource (SPIDR) at "http://spidr.ngdc.noaa.gov/spidr". The 10.7 cm solar flux is an alternative estimate of solar activity. It is a measure of radio emission from the Sun at a wavelength of 10.7 cm (f = 2.80 MHz). If either SSN or F10.7 cm is chosen as the preferred index, then ASAPS converts the value to a T-index when computing the prediction (Advanced Stand Alone Prediction System (ASAPS) Manual, 2008).

The antennas database of ASAPS contains the files of the gain patterns for two-dimensional (2D) and three-dimensional (3D) antennas. The 2D antennas require gains for take-off angle and frequency combination and are considered to be omnidirectional. The 3D antennas require an additional gain for the bearing combination. Antenna gains in ASAPS are expressed in dBi. All gains for different take-off angles and frequencies are referenced to a theoretical isotropic antenna which radiates energy equally in all directions.

3.4.4 Output parameters

The output parameters depend on the ASAPS version used. In this project, two versions of ASAPS were used, 2.0 and 5.1. ASAPS V5.1 contains all the parameters which V2.0 has and therefore only V5.1 is presented here. The output parameters are :

Best usable frequency (BUF), Estimated power required, Field strength, Gains, Height, Losses, Noise field strength, Noise pathloss, Probability, Signal-to-Noise, and Take-off angle.

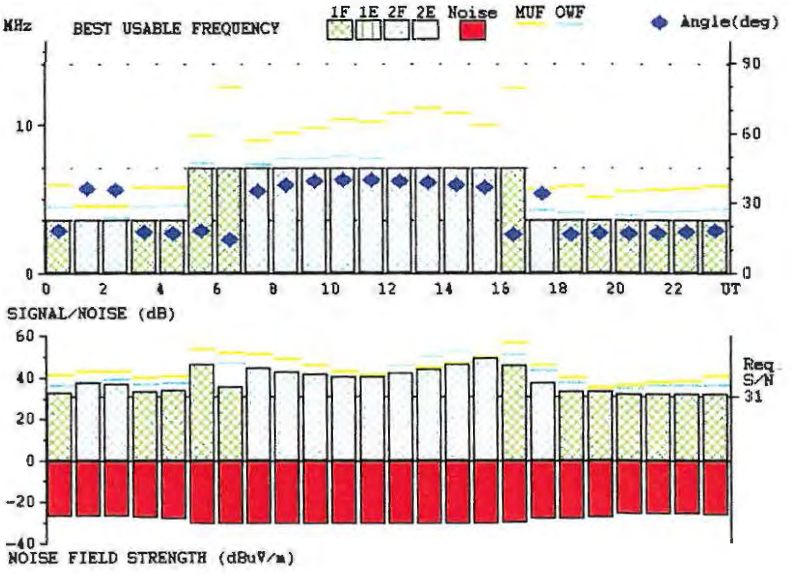

Figure 3.8: The field strength prediction graph shows different output parameters: BUF, OWF (Optimum Working Frequency), MUF, Angle, SNR and Noise field strength.

Figure 3.8 shows the propagation for the Pretoria-Hermanus path within South Africa. This figure represents different modes of propagation as 1F, 1E, 2F and 2E. For example, the signal propagating from about 8:00 to 16:00 UT was reflected by two hops in the F layer, 2F. It also shows the take-off angle at which the signal was transmitted (blue diamonds) in figure 3.8. The SNR is represented in the lower panel of figure 3.8 and the y-axis of the right hand side shows the minimum required SNR which was set as an input value. A minimum SNR is required to maintaiu a desired grade of standards.

Figure 3.9 represents the area prediction results for 16:00 UT only with a transmitter located in Grahamstown, South Africa. The figure shows the frequencies which are possible for transmission within certain areas at a particular time. The South-East part of Africa shows the BUF to be 7 MHz and as the propagation moves towards central Africa the BUF increases to 14 MHz. Thus, for a particular time, the frequency used differs with latitude.

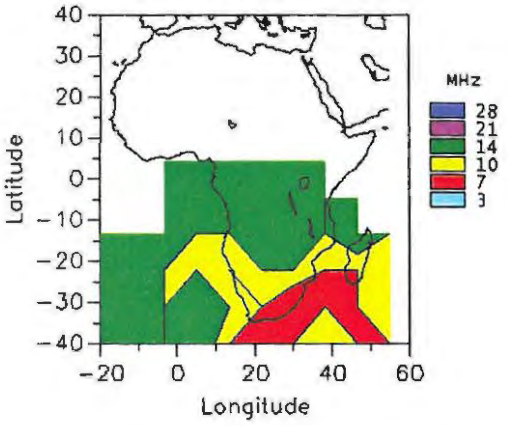

Figure 3.9: The Best Usable Frequency (BUF) graph at 16:00 UT over the African region.

3.5 Antenna Effects in HF Propagation Models

The antenna is one of the important parameters in HF propagation. There are many factors to consider when designing these antennas for inclusion in the models. The mounting location, the height above the ground and a good ground for the antenna are the important factors which may affect propagation. The ground conductivity at one location may differ at another site and therefore, the antenna should be far removed from conductive objects such as power lines, phone wires and gutters. The ground conductivity has a direct effect on the variation in the impedance versus height of the antenna above the ground (Hutchinson, 1985). The ground conductivity refers to the electrical conductivity of the subsurface of the Earth and the impedance is determined by the ratio of voltage to current at the feed point to the antenna.

3.5.1 Basic antenna parameters

There are antenna parameters which play a role in the signal effect transmitted or received. Some of these parameters are radiation pattern, directivity and gain of the antenna. Figure 3.10 is an example of an antenna radiation pattern with main lobe and minor side lobes. The main beam pattern is where the maximum radiation power is obtained and there is low radiation power from the side lobes.

The bandwidth of an antenna refers to the range of frequencies over which the antenna can be used to obtain good performance.

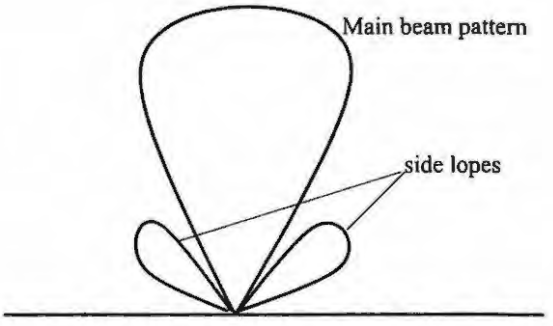

Figure 3.10: An example of the antenna beam pattern with two side lobes.

The radiation pattern changes with frequency. Therefore, the radiation power transmitted or received depends on the frequency used. An example is shown in figure 3.11 of radiation patterns for the G5RV antenna generated by EZNEC which is antenna software that uses numerical electromagnetic code (NEC) for antenna analysis (Carr, 2001b). The four graphs shown have different frequencies and these represent the change in radiation pattern with frequency. These changes in radiation pattern have effects on the signal strength.

There are two types of antennas : directional and omni-directional antennas. The omni-directional antenna radiates energy in all directions while the directional antenna radiates in a particular direction. The concept of directivity and antenna gain are of concern when building an antenna. Directivity is a measure of how focused an antenna coverage pattern is in a given direction. Certain directions are favoured, others rejected and this is how the antenna acquires gain (Carr, 2001a).

The directional gain of an antenna is the ratio of the radiation power in a given direction to the power that would be produced by a hypothetical ideal antenna that radiates equally in all directions (isotropic). The power gain is measured in

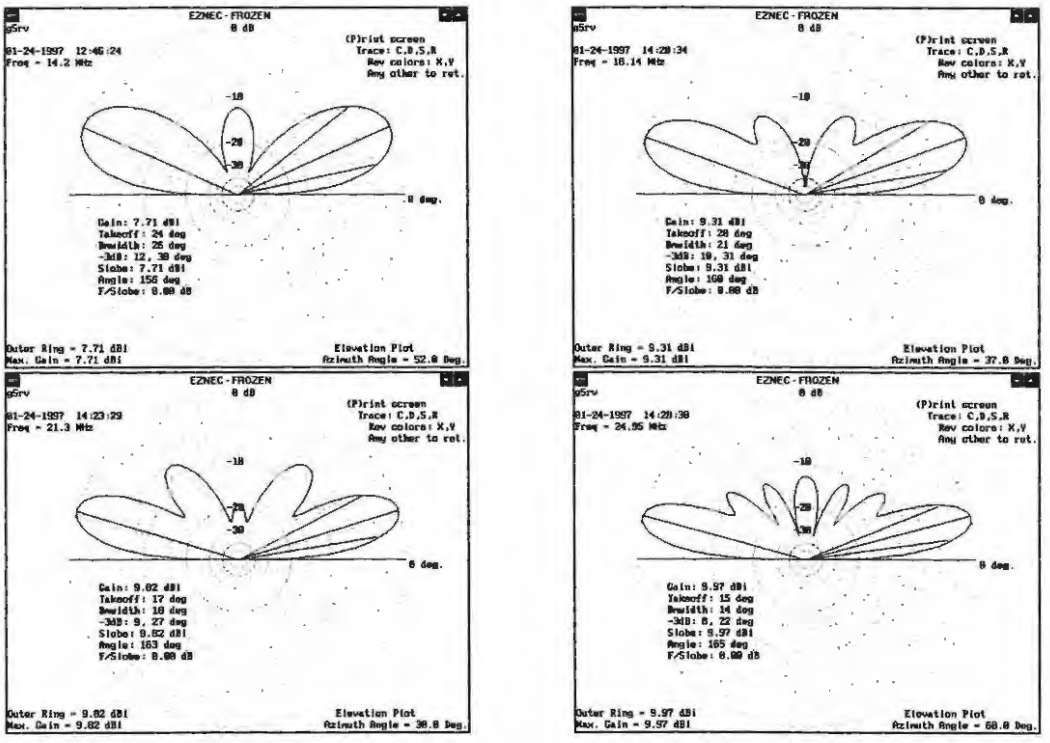

Figure 3.11: Antenna radiation patterns for the G5RV antenna with different frequencies generated by EZNEC obtained from http://www.qsl.net/k2hq/g5rv.htm.

decibels (dB). The equation for the power gain in decibels is given by:

$$G = 10log\left(\frac{P_{out}}{P_{in}}\right) \tag{3.2}$$

where P_{in} and P_{out} is the input and output power and G is either power gain or power loss. The positive value of G in equation 3.2 represents the power gain whereas the negative value of G represents the power loss. A result of "0 dB" means that the ratio of the signals is 1:1, thus there is no gain or loss of signal strength (Carr, 2001a).

Antenna polarization

Polarization is a property of waves that describes the orientation of their oscillation. Mostly the HF-band antennas are either vertically or horizontally polarized. Polarization is determined by the position of the radiating element or wire with

respect to the Earth's surface. Thus, a radiator that is parallel to the Earth's surface radiates horizontally; while an antenna perpendicular to the Earth's surface radiates a vertically polarized wave. During line-of-sight communication, the received signal strength will be a maximum when both antennas have the same polarization. If the transmitter and receiver antennas have different polarizations the received signal strength will decrease.

3.6 Summary

ICEPAC and ASAPS prediction models are important for HF propagation prediction over Africa although they were not specifically developed for the African region. There are many input parameters to set in these prediction models. Some of these parameters have a large effect on the prediction output which in turn affects the accuracy of the results. Therefore, it is important to set them correctly referring to equipment used for real time measurements.

The main differences between the ICEPAC and ASAPS models that may greatly influence HF propagation predictions are associated with indices and coefficient parameters. The ICEPAC model's indices are Q_e and SSN representing geomagnetic and solar activities respectively while the ASAPS model (V 5.1) uses the T-index (which is a combination of both geomagnetic and solar activities) as the prefered index. With regard to coefficients, the ICEPAC uses the CCIR and URSI 88 coefficient parameters, contrary to ASAPS model (V 5.1) which does not contain any coefficient parameter.

The prediction performance of these models is also strongly dependent on the ionospheric behaviour and this is stored in the form of coefficients. Thus, the coefficients have control over the ionospheric structures and this may be the major factor that accounts for the differences in ICEPAC and ASAPS prediction results.

Chapter 4

Initial Attempts

4.1 Introduction

The previous chapter described the two propagation models which were used in this project. This chapter describes the initial attempts undertaken towards validating ICEPAC over the African region. This chapter describes different ways that were looked at in an attempt to validate these models. To validate the HF propagation models over Africa and assess their performance, real time measurements over the African region are required. The data source for real time propagation available at the start of the project was from the SA 40 meter (40m) Beacon Project. The use of ray-tracing was also considered to determine the possible usable frequencies in certain areas.

4.2 Validation of ICEPAC Model using the South African 40m Beacon Project

The 40m beacon project is a system of beacon transmitters on the 40 meter band operating on a single frequency (7.023 MHz). These beacon transmitters send a signal at 40 milliwatts (mW) transmitting power, and were designed to provide a convenient tool for amateur radio, ionospheric research and educational science outreach. In this project the data from these beacons was used for ionospheric research. The beacons are hosted in different locations within South Africa. Although the HF propagation model needs to be validated over the entire African

Date	Time	Receiver location	Beacon callsign	Signal strength
08-10-2007	10:15	KG43EU	ZS6SRL	S6
10-10-2007	04:10	KG32IB	ZS6SRL	S6
11-10-2007	11:40	KG33XV	ZS6SRL	S5
12-10-2007	14:05	KG43AX	ZS6SRL	S1
14-10-2007	13:23	KG43AX	ZS6SRL	S1
14-10-2007	14:00	KG50DJ	ZS6SRL	S1
17-10-2007	19:07	KF26SB	ZS6SRL	S5
20-10-2007	05:53	STRAND	ZS6SRL	S1
24-10-2007	09:00	KG34UC	ZS6SRL	S1
24-10-2007	17:11	KG30BV	ZS6SRL	S9+10
28-10-2007	09:57	KF26SB	ZS6SRL	S1
28-10-2007	10:03	KF26SB	ZS6YI	S1
08-11-2007	13:25	KG43AX	ZS6SRL	S7
08-11-2007	13:33	KG43AX	ZS6YI	S5
09-11-2007	14:23	KG43AX	ZS6SRL	S8
09-11-2007	14:34	KG43AX	ZS6YI	S7
14-11-2007	15:08	JF95FS	ZS1AFU	S3

Table 4.1: The 40m beacon propagation report from different receiver stations.

region, the initial validation attempts were constrained to South Africa.

These beacons transmit signals during different time slots, sending a morse code message also known as CW mode (Dennison and Fielding, 2007). Morse code was developed by Samuel FB Morse in the early part of the 19th century and is a system of dots and dashes that is used to represent letters of the alphabet. These signals can be communicated audibly by telegraph, or visually at night with a blink of a lamp.

Signal strenth reports from these beacons are submitted to the HMO website for analysis by radio amateurs and students volunteers. The reports comprise the incoming signal quality strength measured in S-meter units, the transmitter and receiver location indicated by call signs, and the time slots, as shown in table 4.1.

A brief description of the S-meter units is given by Laster (2000). The S-meter indicates the relative strength of the incoming signal and can be described as follows:

S1 - Faint signals, barely perceptible.
S2 - Very weak signals.
S3 - Weak signals.
S4 - Fair signals.
S5 - Fairly good signals.
S6 - Good signals.
S7 - Moderately strong signals.
S8 - Strong signals.
S9 - Extremely strong signals.

The predicted SNR in ICEPAC is measured in dB and in table 4.1 the data is given in S-meter units. Therefore, to correlate predicted and measured SNR the measured values from the S-meter need to be converted to dB units.

The process of converting S-meter values into SNR in dB.

The beacons transmit in CW mode on the 7.023 MHz frequency. The S-meter readings determine the signal strength without noise included. To compare S-meter readings with SNR, the noise power level has to be included. The noise power is given by

$$P_n = F_a + B - 204 \tag{4.1}$$

where P_n is the available power in dBW, F_a is the external noise figure in dB and $B = 10log(b)$, with b defined as the noise power bandwidth. The value of the noise power bandwidth b of a CW mode is 300 Hz and therefore B can be obtained from the above expression. At 7 MHz frequency the F_a value is $\sim$ 32 dB as determined by International Telecommunication Union Recommendation: ITU-R (2007). After calculating the noise power in dBW it is converted to dBm using the following equation

$$P_n = 10log\left(\frac{P_1}{1W}\right) \tag{4.2}$$

The value of the noise power was calculated to be P_n = -117 dBm for the galactic noise source. After calculating the noise power P_n and using a given received power in dBm for respective S-meter readings, the S-meterr reading can now be converted

to SNR (dB). The table of the received power for frequencies below 30 MHz was obtained from the website http://www.giangrandi.ch/electronics/radio/smeter/smeter.html. Table 4.2 shows the S-meter reading as converted into SNR (dB) after including the noise powerof -117 dBm.

S-meter	Received power (dBm)	SNR (dB)
S1	-121	-4
S2	-115	2
S3	-109	8
S4	-103	14
S5	-97	20
S6	-91	26
S7	-85	32
S8	-79	38
S9	-73	44
S9+10	-63	54
S9+20	-53	64

Table 4.2: Conversion table of S-meter reading into SNR (dB) by including the noise power of -117 dBm.

The measured data after converting to dB was compared with the predicted data generated by the ICEPAC model for the incoming signal strengths, as shown in figure 4.1. The variation between the measured and predicted values is large. Also, there is no clear pattern for the signal strength in either the measured or predicted values shown in figure 4.1. Due to the non-uniformity within the data and the very small set of data available, the data points are at discrete intervals with different interval ranges.

The scatter plot of the measured and predicted signal strengths is shown in figure 4.2. According to this figure, there is no correlation between the measured and predicted signal strengths. In this case, the sparsity of the available data may be the problem in making any conclusion. In addition, these data points are not consistent with time and may not provide a clear performance of the model.

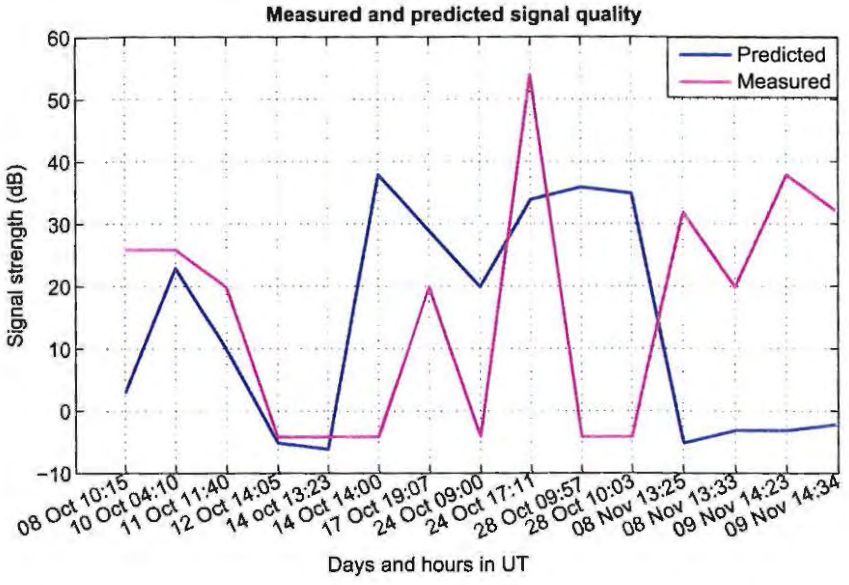

Figure 4.1: The comparison between the measured and the predicted signal strengths in dB from the 8th of October to the 9th of November 2007.

The data analysis done at this stage may have its shortcomings, bearing in mind that the data is submitted by volunteers and data quality can therefore not be guaranteed. The way to obtain enough and consistent data would be to have an automatic beacon monitor which records the incoming signal strength from all the beacon transmitters; however, there is currently no automatic monitor for the SA beacon transmitters. and the method of volunteers sending data to the HMO may not be a good way since data quality may not necessarily be an assurance. Another option is to use a simple ray-tracing programme. This programme provides the signal's propagation path and will be described in the next section.

4.3 Ray-Tracing

A ray-tracing programme can be used to determine a path that a radio signal will follow from a transmitter to a receiver. For this project, a simple ray-tracing programme as described in McKinnell (2002), was used to calculate the ground distance of the propagation path between two locations. This programme uses a file that contains ionospheric parameters which include SSN, the magnetic index

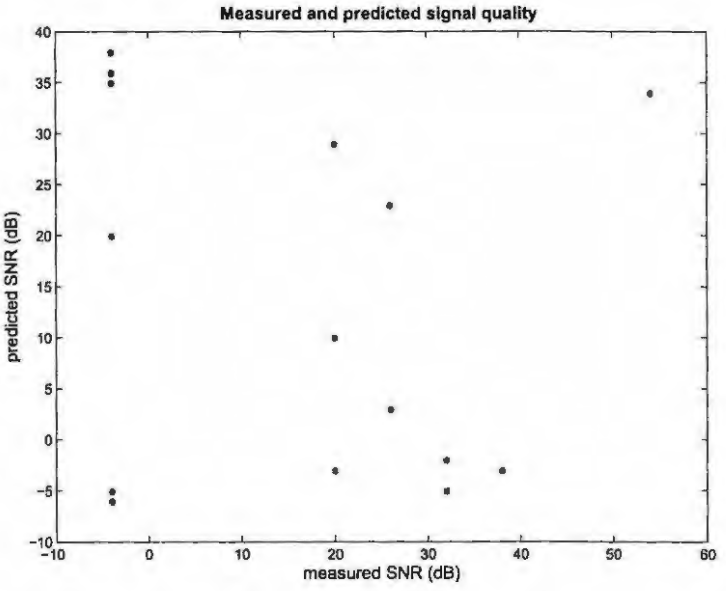

Figure 4.2: This is a scatter plot showing the measured against the predicted signal strengths in dB for the same period as in figure 4.1.

such as Kp or Ap index, plasma frequency, and the height at which the signal is reflected back to Earth. All these parameters can all be obtained from the SPIDR data source except the plasma frequency. The plasma frequency is calculated from the electron density using the following expression :

$$f_c \approx 9\sqrt{N}(MHz) \tag{4.3}$$

where f_c is the plasma frequency and N is the number of electrons per unit volume (McNamara, 1991). The elevation angle and the frequency of transmission are required as inputs when running a programme to calculate the ground distance. Ground distance is the distance along the ground between a transmitter and a receiver. It is measured in kilometers (km) and is obtained for different frequencies at a certain elevation angle, but the elevation angle can also be varied.

For a particular frequency and elevation angle, only one value of the ground distance is obtained. Figure 4.3 is an example which represents a transmitter at point **A** and a receiver at point **B**. The received signal can be at any point along the blue dotted line for a particular input frequency. After obtaining the ground distances

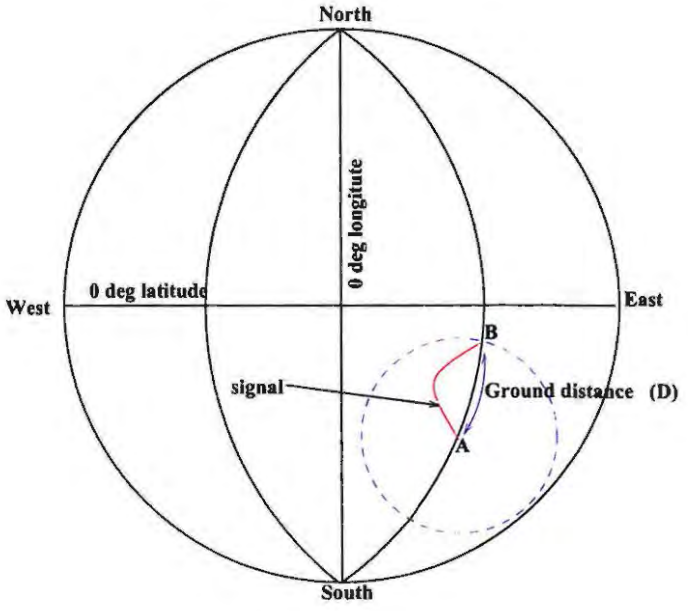

Figure 4.3: The geometric representation of points **B** of reception (on blue dotted line) on Earth to known distance D from point **A**.

for different frequencies their conversion from km to longitude and latitude points is needed. The conversion of longitude and latitude to distance is described by Pearson (1990) who demonstrates the great circle distances. The same idea was applied here to compute the equations which can be used for this conversion.

Figure 4.4 represents a spherical geometry with a transmission point **A** and a receiver in any direction shown by a black dotted line . Equations 4.4 and 4.5 are obtained from the simple geometry in figure 4.4. These equations are used to calculate the longitude and latitude from a known ground distance, D.

$$\left.\begin{aligned} x &= D \times sin(\theta) \\ y &= D \times cos(\theta) \end{aligned}\right\} \tag{4.4}$$

$$\left.\begin{aligned} \Delta\lambda &= \frac{x}{R} \\ \Delta\psi &= \frac{y \times \Delta\lambda}{D} \end{aligned}\right\} \tag{4.5}$$

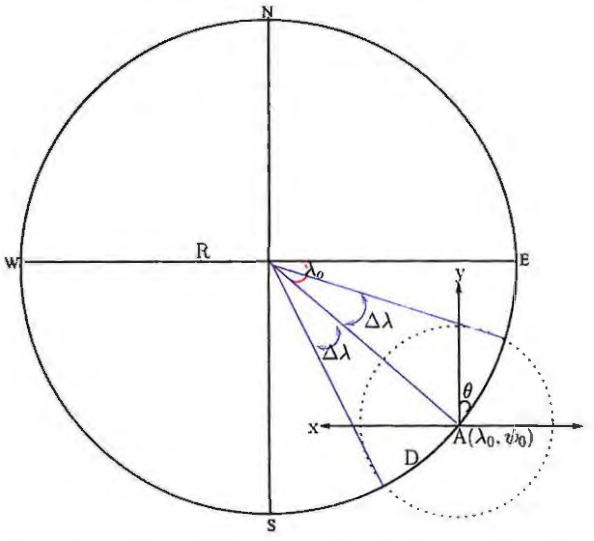

Figure 4.4: The geometric representation of points **B** of reception (on blue dotted line) on Earth at a distance D from point **A**. A point of transmission A is shown in longitude and latitude as $A(\lambda_0, \psi_0)$.

where θ is the elevation angle, D is the ground distance, R is the radius of the Earth, $\Delta\lambda$ and $\Delta\psi$ are changes in longitude and latitude respectively. Using these equations, you can convert your ground distance into longitude and latitude points around a transmitter.

After converting the ground distance data, the graph shown in figure 4.5 was generated. The final results from this process need to be compared to the area predictions generated by the ICEPAC model. For effective comparisons, the results compared should be generated by programmes developed for the same purpose. The ray-tracing programme provides the ground distance which models the ray path for a certain frequency at a certain angle, whereas the area prediction by ICEPAC shows the possible frequencies around the transmitter location. The best would be to use a model which has been designed for the same purpose and has almost similar features. For this reason, another HF propagation model was included and compared with the ICEPAC model.

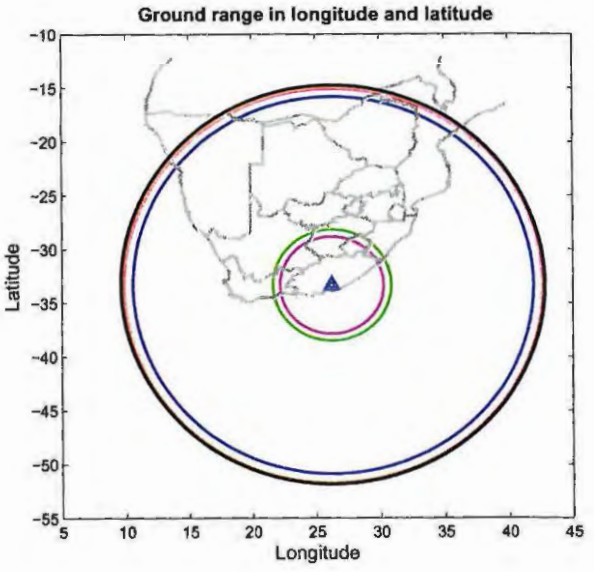

Figure 4.5: The transmitter location indicated by ▲ and the ground distance circles for different frequencies at a 22^o elevation angle.

4.4 ICEPAC Validation by Comparison with Another Model

The comparison of one model with another may not be the best practice for validation, due to the limited availability of real time data, another model had to be used to make the validation. The ASAPS prediction model was suggested as the first choice, since it is highly used by the South African Defence Force. The available ASAPS model considered is version 2.23. The model performs the prediction of frequencies like MUF and FOT (also called the optimum working frequency (OWF)). The output file contains the data for the first and second modes of propagation.

The comparison was made between the ASAPS and ICEPAC frequency prediction for 3 September 2008 for the Cape Town (33.92°S, 18.37°E) to Pretoria (25.75°S, 28.17°E) path within South Africa. The results of the MUF and FOT propagation conditions for first and second modes are presented. The first and second mode of propagation are only presented in ASAPS and not in ICEPAC model. The

ICEPAC model only shows one propagation mode in the output.

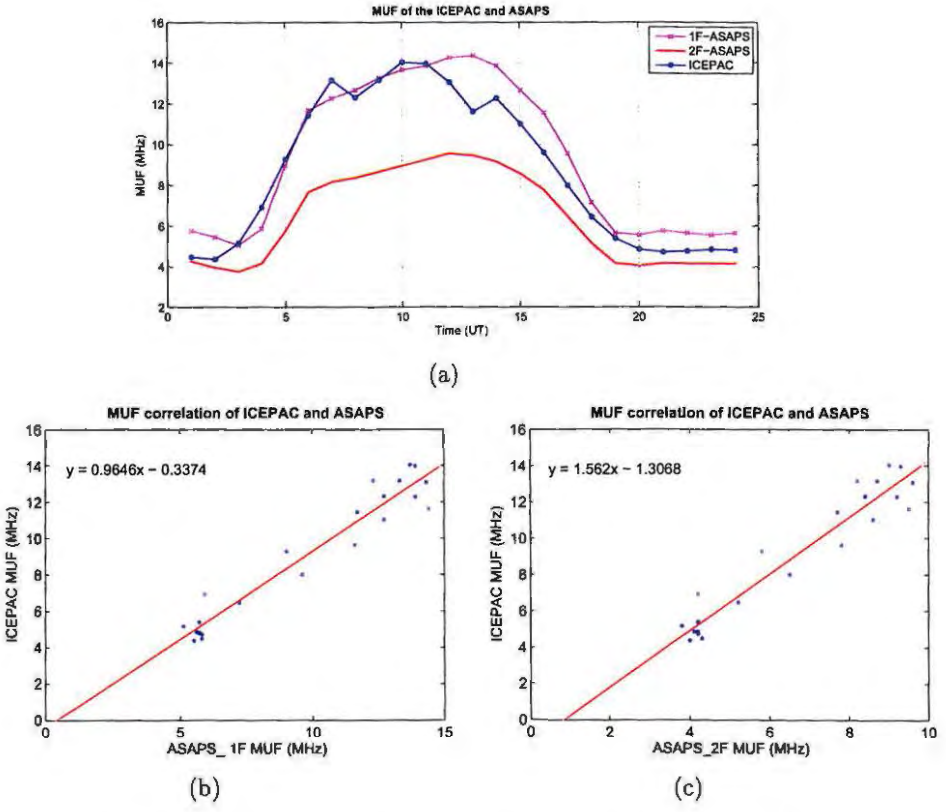

Figure 4.6: Possible MUF values on 3 September 2008 for the Cape Town to Pretoria path. (a) The MUF in MHz plotted against universal time (UT) for the ICEPAC and ASAPS first and second modes. (b) The scatter plot for ICEPAC and ASAPS MUFs first mode. (c) The scatter plot for ICEPAC and ASAPS MUFs second mode.

Figure 4.6 shows the MUF (MHz) for ICEPAC and ASAPS with two modes of propagation. The first mode propagates by a single hop through the F layer and the second mode propagates by two hops through the same layer. Figure 4.6 (a) gives an idea of the maximum frequency that can be used throughout this particular day for the Cape Town-Pretoria path. During the period from 6:00-16:00 UT the frequency is high, whereas for the period before dawn and after dusk the frequency decreases. This is because the electron density is high during the day and

therefore requires higher frequencies for communications (see chapter 2). Figures 4.6 (b) and (c) show scatter plots of the ICEPAC MUF values with corresponding ASAPS MUF values for 1F and 2F modes. Equations of best fit displayed on the scatter plot of figures 4.6(b)-(c) and 4.7(b)-(c) indicate that on average, MUF and FOT values of ICEPAC are less than the predictions generated by the ASAPS first and second modes.

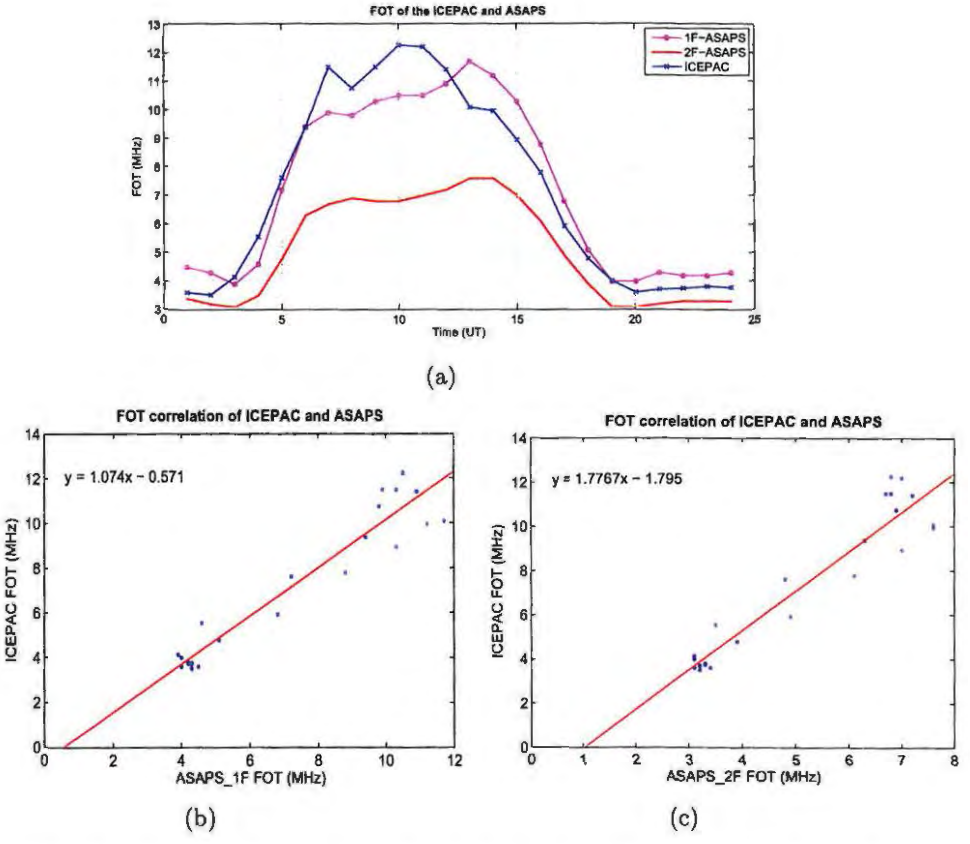

Figure 4.7: Possible FOT values on the 3 September 2008 for the Cape Town to Pretoria path. (a) The MUF in MHz plotted against universal time (UT) for the ICEPAC and ASAPS first and second modes. (b) The scatter plot for ICEPAC and ASAPS FOTs first mode. (c) The scatter plot for ICEPAC and ASAPS FOTs second mode.

The comparison of the FOT (MHz) values of the ASAPS and ICEPAC models is shown in figure 4.7. This figure provides information on the best frequency to use

when communicating along this path. From figure 4.7(a) it is clear that during the daylight hours higher frequencies are required than during the night time hours, which is similar to the observation from figure 4.6 (a).

The computed correlation coefficients, tabulated in table 4.3, from figures 4.6(b)-(c) and 4.7(b)-(c) show that the first mode ASAPS has slightly higher correlation than the second mode ASAPS. However, both modes of ASAPS correlate fairly well with ICEPAC. The question arises as to which model provides the more accurate predictions over the African region. The performance of these two models over the African region may not be well understood without comparison with the real time propagation conditions.

	ICEPAC + ASAPS 1F	ICEPAC + ASAPS 2F
MUF	0.9692	0.9631
FOT	0.9576	0.9518

Table 4.3: The correlation coefficient of ICEPAC and ASAPS for first and second modes. The correlation coefficients of the MUF and FOT are presented.

The only way to accurately collect real time propagation data is to set up an automatic beacon monitor. The 40m beacon project was put on hold in January 2009 and at that stage did not include an automatic beacon monitor. Therefore, there was no possibility of accessing more data from this project and an alternative source of real-time data had to be found.

The alternative source of real time data proved to be the International Beacon Project (IBP). A real time HF beacon monitoring station for the IBP is now operational in Hermanus, South Africa (Mudzingwa, 2009). The IBP is a network of beacons located around the world and set to transmit a signal on five different frequency bands. The International Beacon Monitor measures the incoming signal strength for the global stations. The monitoring station started collecting the data towards the end of August 2008 for a single frequency bandwidth (14.1 MHz). The multiband receiver started collecting data in mid-December 2008 for all five frequency bands.

The use of real-time measurements are the only way to evaluate the performance of the models. Since the real-time data measurements became available, proper validations of the models became possible. For the rest of this thesis the ASAPS model continues to be used together with ICEPAC to investigate the performance of both models when compared to real-time propagation data.

Chapter 5

Performance of HF Propagation Models

5.1 Introduction

This chapter presents the validation of the HF propagation models. The real-time measurements were obtained from the International Beacon Broject. Two international beacon transmitter stations were considered : Ruaraka, Kenya (1.24°S, 36.88°E) and Pretoria, South Africa (25.45°S, 28.10°E). Only one receiver station was used, namely Hermanus, South Africa (34.27°S, 19.12°E). These stations were chosen because they fall within the African region of interest. In this chapter the input parameters of HF propagation models which may be necessary to predict HF propagation paths over Africa are described, as well as the test results with regard to the antennas, the chosen indices (SSN, effective SSN, T-index and F10.7 cm). The International Beacon Project is also discussed.

5.1.1 Antenna effects

Antennas are divided into two categories, namely directional and non-directional. Directional antennas favour a definite direction of radiation, while non-directional antennas do not follow any particular direction (Carr, 1993). The antenna can either be in an elevation or azimuthal direction. Elevation refers to the angle between the dish pointing direction and the local horizontal plane. Azimuth refers to the rotation of the whole antenna around a vertical axis. Both the azimuth and

elevation angles can have effects on the signal. This section presents the effect of elevation angle on signal strengths for directional and non-directional antennas. The isotropic antenna was used as the non-directional (figure 5.1(a)) and a tropical array was used as the directional (figure 5.1(b)) antenna, since the radiation patterns of the isotropic and tropical array antennas represent the non-directivity and directivity of the radiation power respectively.

The ICEPAC model was used to predict SNR values for directional and non-directional antennas to assess their effects on the signal strength of a radio signal along a particular path. The SNR values are plotted against elevation angle for both directional and non-directional antennas as shown in figures 5.1(a)-(b). The non-directional antenna used for the situation shown in figure 5.1(a) radiates equally in all directions and therefore, changing the direction of the antenna by varying the elevation angle will not have any effect on the signal strength. Figure 5.1(a) shows the signal strengths for six different frequencies with elevation angles on the x-axis. The SNR values remain unchanged throughout different elevation angles, since the radiation energy is the same in all directions despite the change in elevation angle.

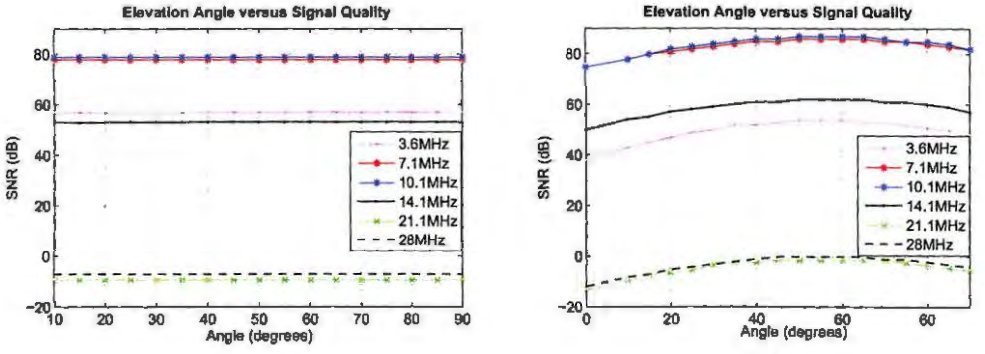

(a) (b)

Figure 5.1: The directional and non-directional antenna effects on SNR values for varying elevation angles at different frequencies.

The directional antenna (transmitter) used in figure 5.1(b) has, however, maximum radiation in the direction of the receiver. If the maximum radiation of a receiver antenna is pointing in the direction of a transmitter, then a strong signal can be

received. But if the receiver antenna is pointing in the opposite direction, this may lead to a weak signal (but quite likely no signal) being received. The SNR values (in figure 5.1(b)) change with elevation angle and therefore, the direction of an antenna in this case is important for the effect it might have on the signal.

5.1.2 Indices for the ICEPAC model

The HF propagation predictions can be performed by either using SSN or effective SSN indices. In this section both indices are used as test inputs for the prediction of SNR values. The HF propagation predictions were done for four days of September 2008 in order to graphically compare the SNR output values given by the two indices as shown in figure 5.2. The SSN provides higher predicted SNR values than effective SSN for all four days considered. The average difference between SNR values obtained using SSN and effective SSN as input, is between 7 to 8 dB. The foF2 data used to calculate the effective SSN was obtained from the Grahamstown ionosonde station (33.32°S, 26.50°E), since the propagation path considered is across Africa.

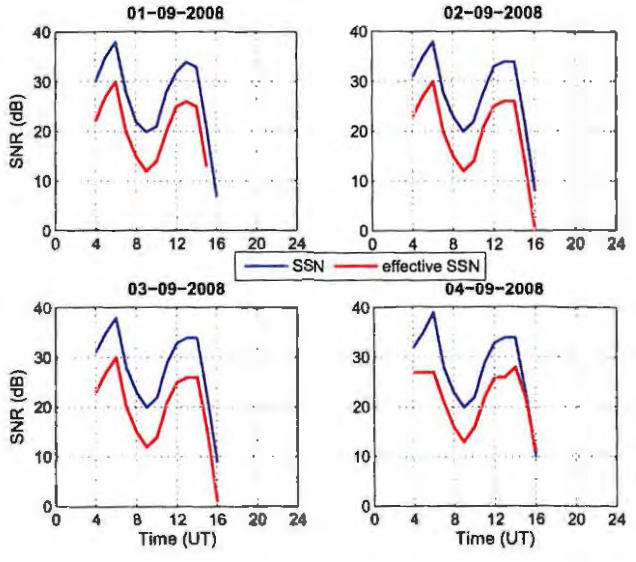

Figure 5.2: HF propagation prediction of SNR values using SSN and effective SSN for four days during September 2008, across Africa.

5.1.3 Indices for the ASAPS model

The HF propagation predictions using ASAPS were made using the T-index, although there are other indices that can be used for this model, such as SSN and F10.7 solar flux. The T-index is preferred for the ASAPS model, since it includes solar and geomagnetic activities. It can be obtained from the South African Space Weather website (Kobus Olckers, 2009, http://www.spaceweather.co.za/). Figure 5.3 shows the predicted SNR values using ASAPS model with three indices as inputs: T-index, SSN, F10.7 solar flux.

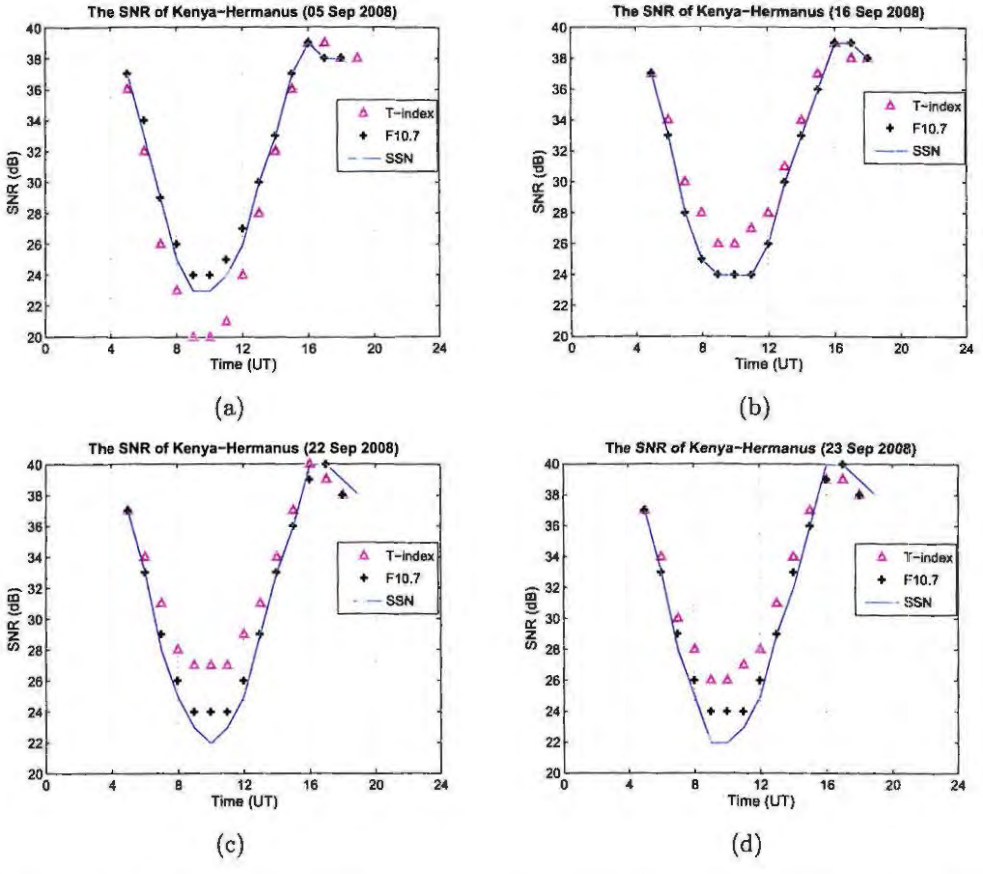

Figure 5.3: The predicted SNR values along a propagation path across Africa using ASAPS with three different indices, namely T-index, SSN and F10.7 solar flux, for four days during September 2008.

The predicted HF propagation SNR values using the SSN are lower than those

resulting from the use of the T-index and F10.7 solar flux indices. The values of T-index used for the prediction were negative values, except for the value used in figure 5.3(a). The negative value of the T-index indicates that there is low ionospheric activity. The positive value of the T-index used in figure 5.3(a) caused the SNR values to decrease to about 6 dB on average between 8:00 and 12:00 UT as compared to the other results shown in figures 5.3(b)-(d). The predicted SNR values are almost the same for all three indices, except for the predictions between 7:00 and 13:00 UT where a difference of about 2 dB can be observed.

5.1.4 International Beacon Project results

The International Beacon Project (IBP) is a worldwide network of beacons constructed by the Northern California DX Foundation (NCDXF) and the International Amateur Radio Union (IARU). This network of beacons was designed to operate as a worldwide network of HF radio beacons broadcasting on the 14.10, 18.11, 21.15, 24.93, and 28.20 MHz frequencies at a transmitting power of 100 Watts.

The IBP is important for both amateur and commercial HF radio users to assess the current conditions of the ionosphere. These beacons are located across the globe and identified by their call signs as shown in figure 5.4. The call signs written in red, indicate the transmitters which were used for this project together with the receiver call sign in black. These stations were used since the purpose of study is to validate HF propagation models over Africa. These beacons provide real-time HF propagation data from all the transmitter stations to the receiver station, for example, HF propagation data is received from 5Z4B at ZS1HMO.

The 5Z4B (Ruaraka) beacon uses a TS50 modified by NCDXF for frequency control and timing by GPS. The antenna is a Cushcraft R5 vertical set about 10 meters above ground, 360 degree coverage. The ZS6DN (Pretoria) beacon have a cluster of stacked 2x5 elm 6 meters Yagi Arrays.

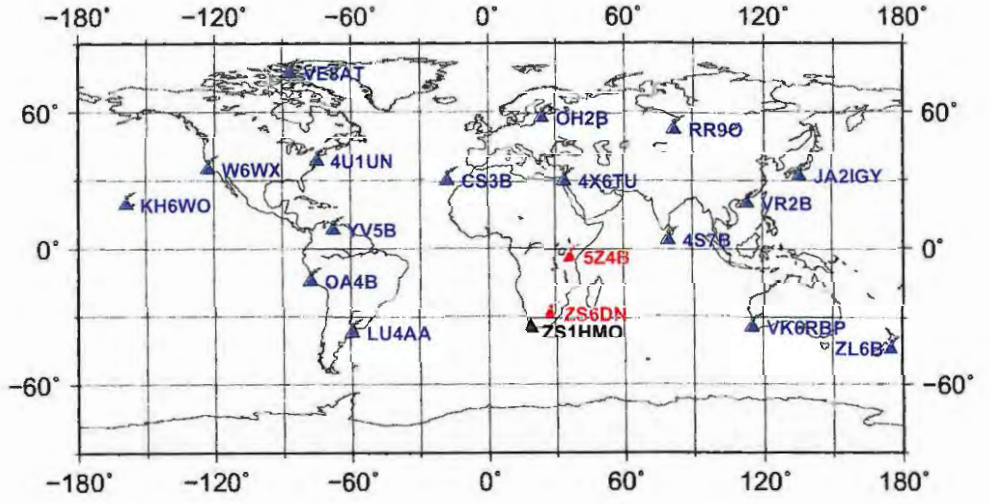

Figure 5.4: Map of the international beacon transmitter locations and the Hermanus receiver station, identified by call signs.

The IBP provides the following parameters as an indication of the real-time propagation conditions: "SNR", "QSB", "Evidence" and "Delay". The "SNR" parameter provides an indication of the signal strength, and the "QSB" parameter represents the fraction of time when the signal was below the noise. The "Evidence" parameter is a probability measure, indicating the probability of a beacon transmitted signal being received, with a threshold set to Evidence = 1. An evidence of 1 indicates the highest possibility of a particular transmitted signal being received. The "Delay" parameter provides the time interval in milliseconds between the start of the transmitted signal to when the signal is received (De Canck, 2006a). For this project only the "SNR" parameter was extracted for analysis.

The values of the measured SNR are plotted against time for both the single frequency, as well as the multiple frequency cases shown in figures 5.5 and 5.6 respectively. The monitoring station (ZS1HMO) started collecting propagation data towards the end of August 2008 on a single frequency (14.1 MHz) band and, thereafter, a multiband receiver was installed which started collecting data in mid-December 2008 for all five frequency bands (Mudzingwa, 2009).

In this project the paths from Ruaraka, Kenya (1.24°S, 36.88°E) to Hermanus, South Africa (34.27°S, 19.12°E) and from Pretoria, South Africa (25.45°S, 28.10°E)

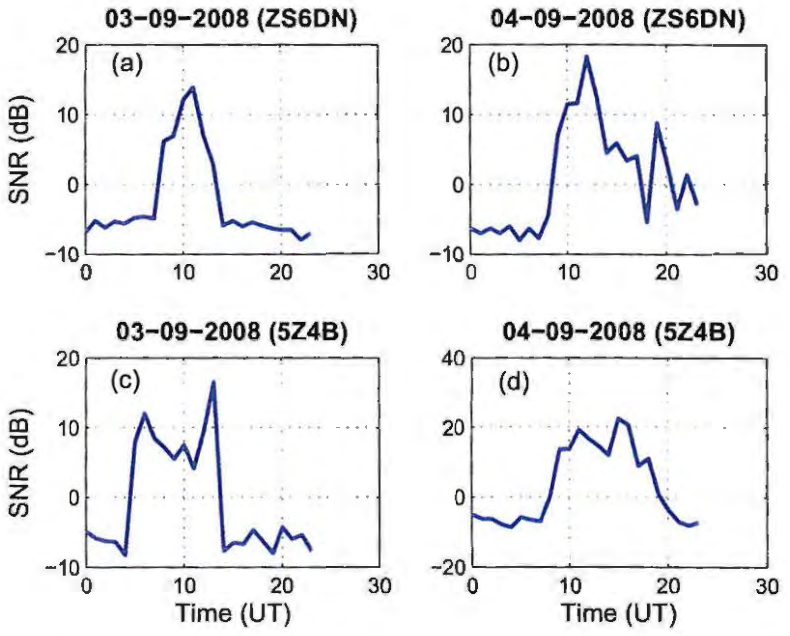

Figure 5.5: The measured SNR for single band propagation over the ZS6DN and 5Z4B paths.

to Hermanus are defined as 5Z4B and ZS6DN respectively. Figure 5.5 represents the measured SNR values for the 14.1 MHz frequency band for two days within September 2008 across both paths. The morning and afternoon hours have negative SNR values, while the positive SNR values were obtained during the daytime hours from about 7:00 to 14:00 UT for ZS6DN (figure 5.5 (a)-(b)) and 5:00 to 18:00 UT for 5Z4B (figure 5.5 (c)-(d)). The negative SNR values mean that the signal power is below the noise power. Therefore, reliable communication may not be possible unless steps are taken to increase the signal power or reduce the noise level of the receiver (Doberstein, 2009).

The same scenario was observed for multiband frequency plots shown in figure 5.6, where the variation of SNR values for five different frequencies along the two considered paths are shown. The measured SNR values in figure 5.6 for some frequencies (e.g 24.9 and 28.2 MHz) have negative values for both the ZS6DN and 5Z4B paths. In general, the SNR values are lower and become negative for higher frequencies.

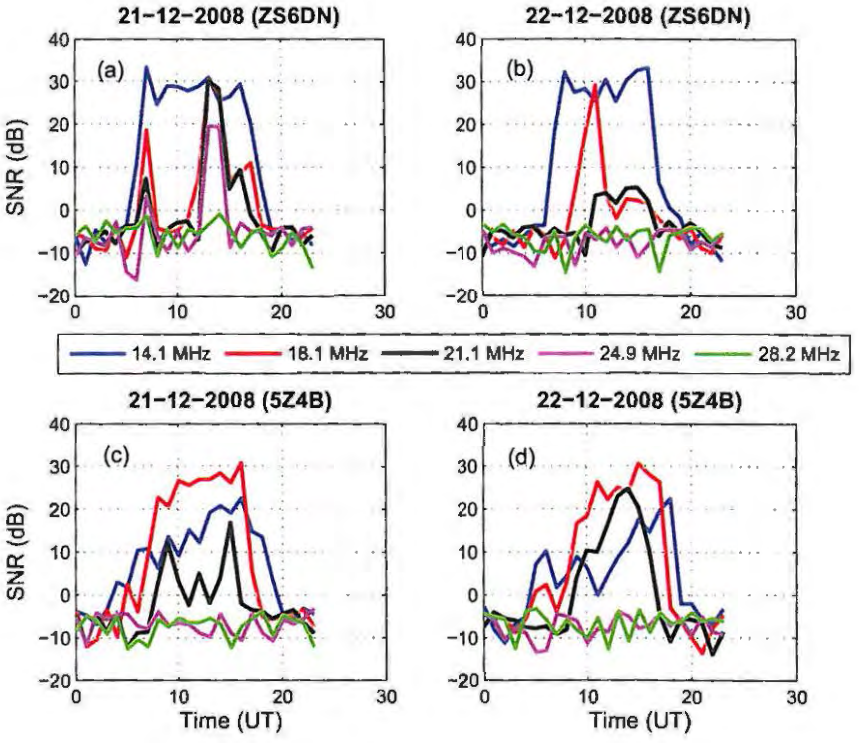

Figure 5.6: The measured SNR for multiband propagation along the ZS6DN (a - b) and 5Z4B (c - d) paths.

In figure 5.6 (a)-(b) SNR values are higher for 14.1 MHz, whereas in figure 5.6 (c)-(d) the higher values of SNR are for the 18.1 MHz frequency band. This indicates that the 14.1 MHz frequency is the optimum frequency for the ZS6DN path, whereas 18.1 MHz is the optimum frequency for the 5Z4B path. It also indicates that low frequencies are good for short-distance communication and, as the distance of communication between two points increases, higher frequencies may be used. Please note that this observation is only valid for the dates that were used in this preliminary analysis and different results may be expected for other times of the year.

5.2 Introduction to Performance of the Models

Recently, a study was done to assess the performance of the ICEPAC model using the MUF propagation parameter over Central Europe (Zolesi *et al.*, 2008). ICEPAC can be used as a long-term prediction model (Zolesi *et al.*, 2008). The oblique ionospheric radio sounding measurements were considered for the paths between Inskip, UK (53.5°N, 2.5°W) and Rome, Italy (41.8°N, 12.5°E) and between Inskip and Chania, Greece (35.7°N, 24.0°E) for periods which fell within the declining phase of the solar cycle 23 (2003 and 2004).

In this project a similar study is done for the paths within the African region (from Ruaraka to Hermanus and from Pretoria to Hermanus). The IBP measurements of the SNR is used for the propagation performance of ICEPAC model. The predictions were made for the period between September 2008 and June 2009, which is a period of minimum solar activity.

The data used for analysis relate to the equinox and solstice months and days, since the major seasonal changes are observed during these periods. The available data obtained prior to December 2008 is for a single frequency band, 14.1 MHz, and therefore, this particular frequency is used for graphic analysis. The SNR data obtained for both the measured and predicted cases contain some positive and negative SNR values. Since the negative SNR values indicate the likely absence of the signal, negative values are excluded from this analysis and the monthly median was calculated for only positive SNR values.

5.2.1 Analysing predicted SNR values by ASAPS and ICEPAC

In this section the monthly median predicted SNR values by ASAPS and ICEPAC are compared to measured data. Data for three months was used for this comparison and the results are shown in figures 5.7(a) - (c). To statistically compare the performance of the two models with respect to real-time data, the root mean square error (RMSE) values were calculated as follows;

$$\mathrm{RMSE} = \sqrt{\frac{1}{N}\sum_{i=1}^{N}(R_s^m - R_s^p)^2} \tag{5.1}$$

where N is the number of data points, and R_s^m and R_s^p are measured and predicted SNR values respectively. The computation of RMSE and correlation coefficients are widely used to estimate the accuracy of data-driven models (e.g Zolesi *et al.*, 2008; Habarulema *et al.*, 2009).

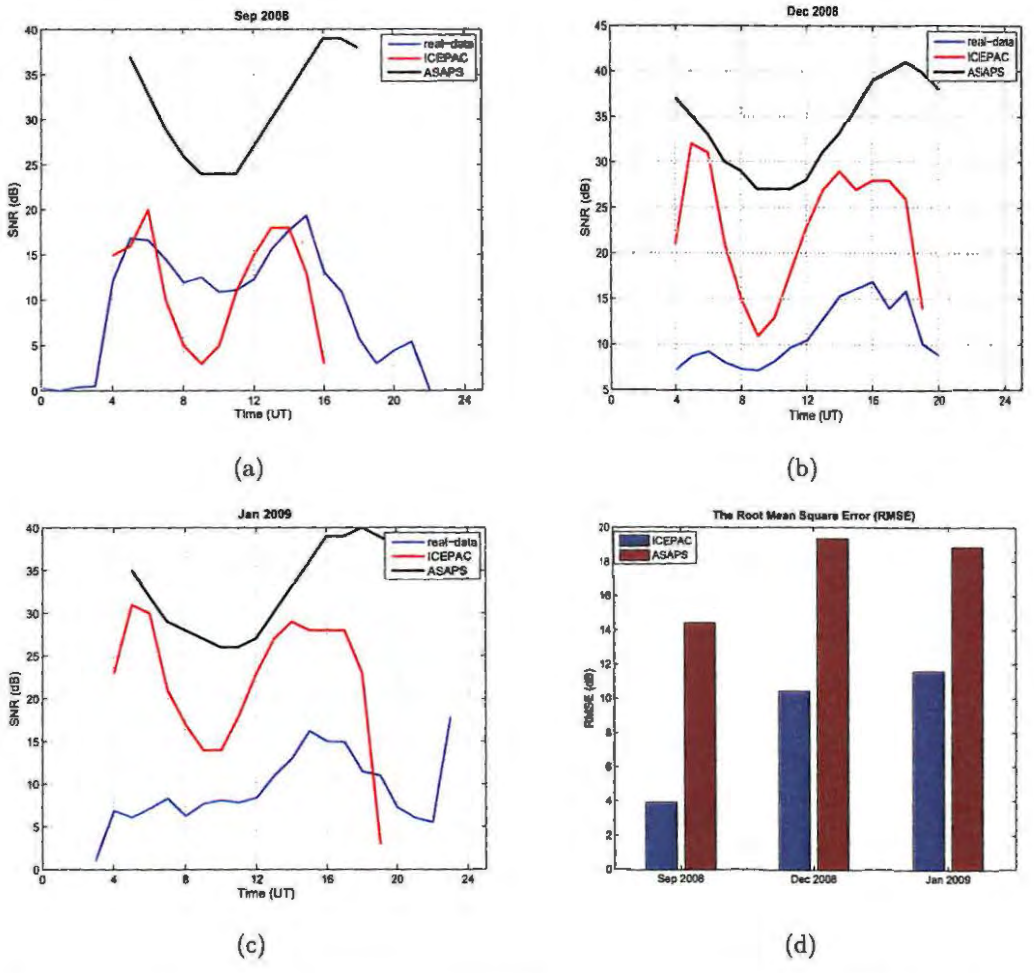

Figure 5.7: The monthly median predictions of SNR values by ASAPS and ICEPAC are compared to real-time measurements in the (a), (b) and (c) panels. The RMSE of ASAPS and ICEPAC for three months are compared in panel (d).

The predicted SNR values analysed in this subsection are for the 5Z4B path at 14.1 MHz by ASAPS and ICEPAC models as shown in figure 5.7(a) - (c). The SNR

values predicted by ASAPS are much larger than the ones predicted by ICEPAC. The SNR values predicted by ICEPAC, however, have low values of SNR during certain daytime hours (approx 7:00 - 12:00 UT). The measured SNR values are on average lower than both the ASAPS and ICEPAC prediction values.

A comparison of the RMSE values computed is shown graphically in figure 5.7 (d). The ICEPAC model seems to provide greater prediction accuracy than ASAPS for the months selected. The large differences between the ASAPS and ICEPAC models are to be expected, since the antennas used in the respective software were not the same and therefore results do not necessarily indicate poor performance by ASAPS. For ASAPS, theoretical isotropic antennas were used at the receiver and transmitter locations, whereas, more representative antennas were provided to ICEPAC. Therefore, the higher ASAPS predictions are to be expected when compared to those from ICEPAC. Modification of the ASAPS antenna files, comprising elevation angles and gains, was not possible due to difficulties experienced with the version of the software used for this project. Therefore, it was not possible, at this time, to make a definite conclusion regarding the use of ASAPS over the African region. This analysis was provided in this section of the thesis for completeness, however, for the rest of the thesis the ICEPAC model will be used.

5.2.2 Analysis of ICEPAC

Daily HF propagation prediction for ZS6DN and 5Z4B paths

In figure 5.8(a) the measured SNR values is compared with the predicted SNR values to assess the performance of the ICEPAC model in predicting the HF propagation conditions for the 5Z4B path. The figure is plotted with error bars on the measured SNR data, where the error bars are the standard deviations of the real-time measurements. Standard deviation is a statistical measure of variability, and can be used to represent the root mean square (RMS) deviation of the values from their arithmetic mean.

$$\delta = \sqrt{\frac{1}{N}\sum_{i=1}^{N}(R_s - \overline{R_s})^2} \tag{5.2}$$

where δ is the standard deviation, R_s is a measured value, $\overline{R_s}$ is the average mean of the measured values and N is the number of measured data points. The standard deviation was computed for the analysis of real-time measurements compared to ICEPAC predictions.

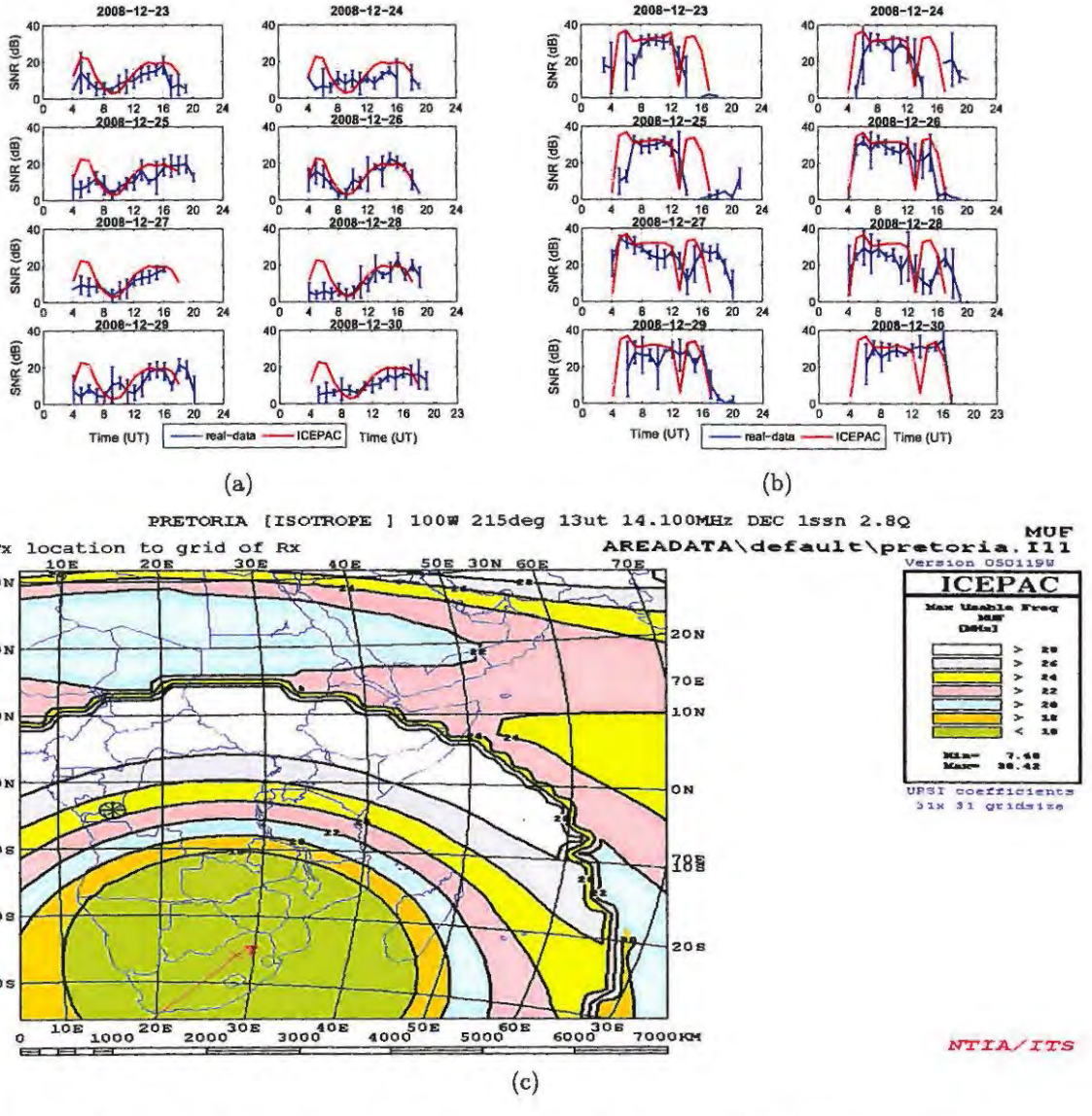

Figure 5.8: The ICEPAC predictions of the SNR values for (a) the 5Z4B path and (b) ZS6DN path for a few selected days in December 2008 and (c) the ICEPAC area coverage for the MUF of the ZS6DN path.

In some cases, results show that ICEPAC predictions follow correctly the daily variation patterns of the measured data. On average the predicted data seems to follow the measured data for certain hours of the day (8:00 - 18:00 UT) as shown in figure 5.8(a). The measured SNR values appear to increase from dawn to dusk which is not the case with the predicted SNR values. The predicted data has high SNR values during the time range 4:00 to 7:00 UT, which corresponds to sunrise at the receiver location, a time when the ionosphere is unstable.

Figure 5.8(b) shows the daily variation of HF propagation conditions for the ZS6DN path. The most noticeable phenomenon in this figure is the sudden decline and increase in the SNR values forming sharp inverted peaks at about 13:00 UT. These inverted peaks are more evident in the predicted than measured SNR values. Figure 5.8(c) illustrates how this effect could be as a result of the skip zone surrounding the receiver location. This figure is the MUF area coverage prediction from ICEPAC for the ZS6DN path.

Comparing figures 5.8(a) and 5.8(b), the 5Z4B path exhibits lower SNR values than the ZS6DN path for this particular frequency and these geophysical conditions. Using the rule of thumb for HF communication, short-distance communication requires lower frequencies and higher frequencies are good for longer distance communication (McNamara, 1991). The minimum frequency used by the IBP is 14.1 MHz and the ZS6DN path would probably have a better signal quality than the 5Z4B path in this case. This observation is the same as made in section 5.1.4, where figure 5.6 showed that for the 5Z4B path there were high values of SNR at 18.1 MHz and lower values of SNR at 14.1 MHz.

The RMSE and correlation coefficient (R) values of the daily HF propagation were computed for the analysis of the ICEPAC model performance as shown in table 5.1. R is defined as

$$R = \frac{1}{\delta_m \delta_p} \left(\sum_{i=1}^{N} (R_s^m - \overline{R_s^m})(R_s^p - \overline{R_s^p}) \right) \tag{5.3}$$

where δ_m and δ_p are the standard deviations for measured and predicted SNR respectively as generally defined in equation 5.2, R_s^m and R_s^p are measured and

Days	RMSE for paths:		correlation coefficients for paths:	
(in Dec 2008)	5Z4B	ZS6DN	5Z4B	ZS6DN
23	6.4065	13.0230	0.6623	0.4734
24	8.1039	14.8111	-0.0245	0.0610
25	5.2337	11.2648	0.4620	0.2440
26	3.9652	8.9355	0.7946	0.7273
27	5.9323	11.6830	0.7230	0.2102
28	7.6611	12.7968	0.3898	0.1884
29	8.2982	9.9547	0.1650	0.3673
30	7.5266	9.2696	0.2958	0.4856

Table 5.1: The RMSE and correlation coefficient values between the measured and predicted SNR for the 5Z4B and ZS6DN paths for selected days during December 2008.

predicted SNR, and $\overline{R_s^m}$, $\overline{R_s^p}$ are their respective mean values. Figures 5.9(a)- (b) also show the RMSE and R respectively for both paths considered.

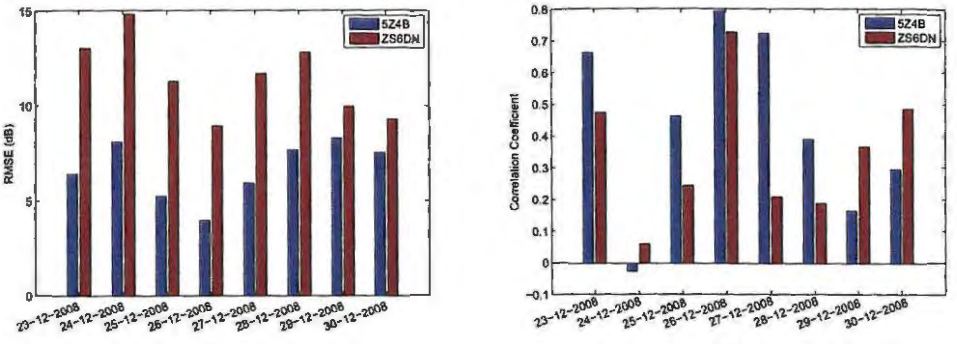

(a) (b)

Figure 5.9: Bar graphs of; (a) the RMSE values, and (b) correlation coefficients (R) of measured and predicted SNR for the paths 5Z4B and ZS6DN during selected days in December 2008.

It can be seen from figure 5.9(a) that on average the accuracy of ICEPAC predictions is better for the 5Z4B path than for the ZS6DN path for the selected days. The computed R also shows a higher correlation for the 5Z4B path in figure 5.9(b) except on days 24, 29 and 30 where it was lower than for the ZS6DN path. Day 24 in figure 5.9(b) shows that the model correlates negatively to the measured data

for the 5Z4B path as evidenced in figure 5.8(a) where the model predicts the opposite of the measured data. The ICEPAC model is a monthly median propagation model, but can also predict daily HF propagation conditions. Therefore, a comparative analysis of the monthly median propagation values between the ICEPAC model and the measured data was also undertaken.

Monthly median HF propagation predictions for the ZS6DN and 5Z4B paths

The monthly variations of HF propagation conditions were considered by calculating the median of all the days in a month for a particular hour. Figures 5.10 and 5.11 represent the monthly performance of ICEPAC propagation predictions of the SNR values compared to the measured SNR values for the 5Z4B and ZS6DN paths.

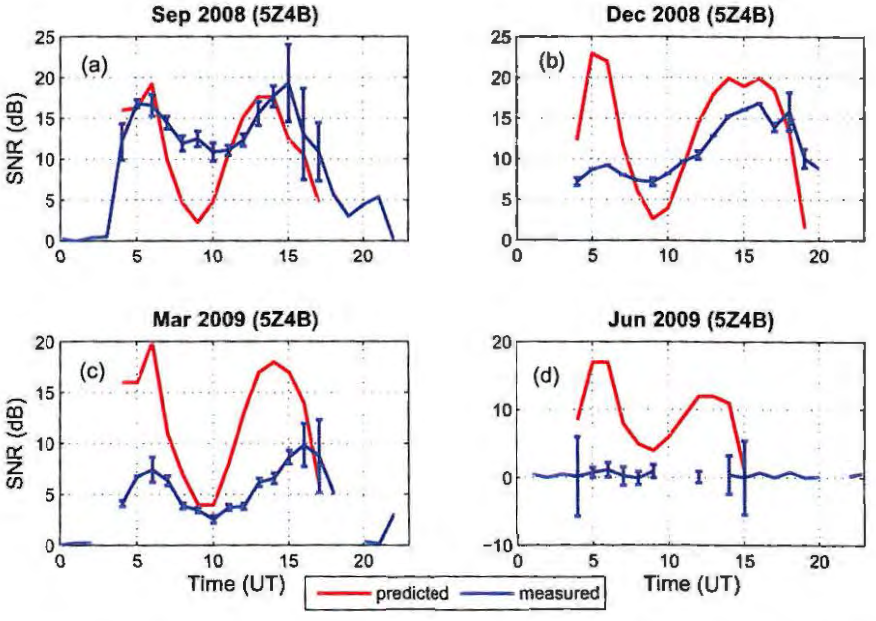

Figure 5.10: The monthly predictions for the 5Z4B path at 14.1 MHz for four months : September 2008, December 2008, March 2009 and June 2009.

The plots (in figures 5.10 and 5.11) of the measured data with error bars of the

standard deviation show the monthly variations of SNR values. Figures 5.10 and 5.11 show a poor performance of the ICEPAC model for both paths. However, the predictions for September 2008 in figures 5.10 (a) and 5.11 (a) appear to follow the measured data for certain hours of the day, for the periods from about 11:00 to 17:00 UT and 8:00 to 16:00 UT respectively. The error bars which represent the standard deviation show that the measured data may vary within the deviation error of a standard value. Therefore, if the predicted SNR value is within or very close to the error bars, then this may generally be considered as good performance of the model.

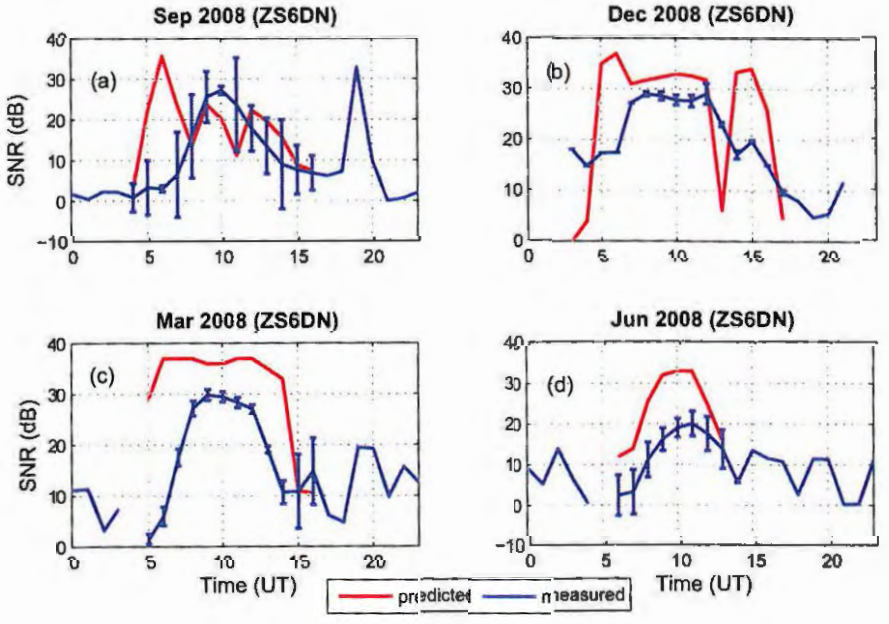

Figure 5.11: The monthly predictions for the ZS6DN path at 14.1 MHz for four months : September 2008, December 2008, March 2009 and June 2009.

Month	RMSE for paths:		correlation coefficients for paths:	
	5Z4B	ZS6DN	5Z4B	ZS6DN
Sep 2008	4.9521	12.5154	0.6275	0.0926
Dec 2008	6.2524	11.9066	0.5381	0.4784
Mar 2009	5.9653	11.5303	0.4952	0.4122
Jun 2008	10.1313	11.5150	0.5501	0.8633

Table 5.2: The RMSE and correlation coefficient of the measured and predicted SNR values for the 5Z4B and ZS6DN paths for four months.

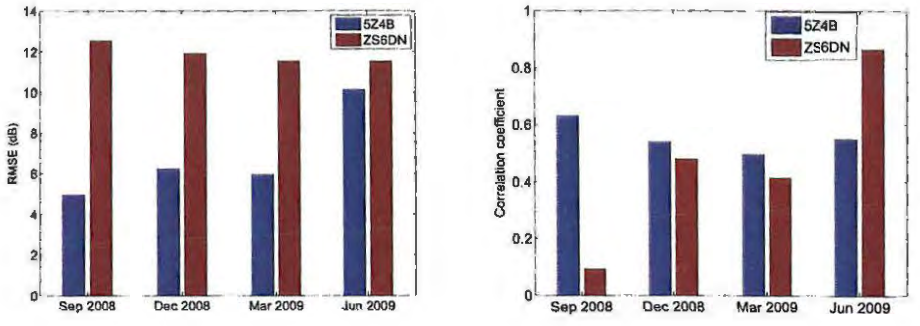

(a) (b)

Figure 5.12: A bar graph indicating the RMSE values (a) and correlation coefficient values (b) for the 5Z4B and ZS6DN paths during the four months.

5.3 The Multiband Frequency Predictions

Figures 5.13 and 5.14 show the performance of the HF propagation models for four different frequencies (14.1, 18.1, 21.1 and 24.9 MHz) along the two African paths. Looking at the possibility of HF communication as indicated by the measured SNR values (figure 5.13 (a)), the available propagation time falls between 4:00 and 17:00 UT. Then, as the frequency increases, shown in figure 5.13 (b), the propagation time narrows to the range between 7:00 - 16:00 UT. The propagation continues to narrow down to a no signal propagation as presented in figures 5.13 (c) - (d). The same phenomena applies in figure 5.14 where propagation is not possible at all in figure 5.14 (d) for the 24.9 MHz frequency band.

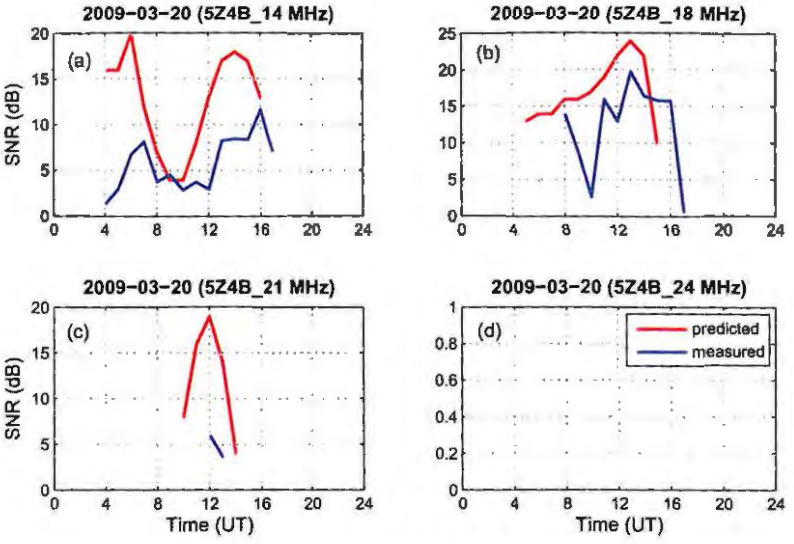

Figure 5.13: The daily predictions for the Ruaraka-Hermanus (5Z4B) path on 20 March 2009.

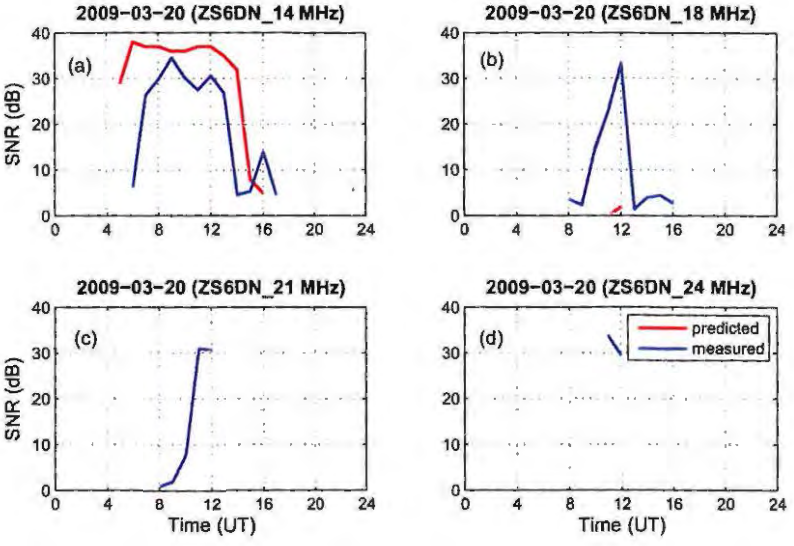

Figure 5.14: The daily predictions for the Pretoria-Hermanus (ZS6DN) path on 20 March 2009.

5.4 Summary

In this chapter the indices which were tested for both the ASAPS and ICEPAC models were discussed and showed a small difference in their performance. Validation of ASAPS and ICEPAC propagation models were performed for the two paths (5Z4B and ZS6DN) over the African region. This was done by using measured data obtained from the IBP. In this study it was found that the ICEPAC model performs more accurately for the daily propagation than monthly median propagation conditions. HF propagation conditions at different frequencies were tested, and more accurate results were obtained over short-distance communication with low frequencies. Therefore, HF propagation at a high frequency may not be possible for short-distance communication. A definite conclusion could not be drawn for the ASAPS model due to the challenges posed by the modification of the antenna file. However, the ICEPAC model was used for the rest of the analysis of the results.

Chapter 6

Conclusion and Future Work

A summary of the results discussed in the previous chapters and possible future work that can be undertaken to extend the validation of HF propagation models are briefly presented in this chapter. The main aim of this project was to validate HF propagation models (ASAPS and ICEPAC) over the African region using data obtained from the IBP. The validations of the HF propagation models were done using for only two paths with available measured data. The ability of the HF propagation models to predict propagation conditions across Africa were studied and analysed in terms of the strength of the signals using the SNR parameter. In terms of the performance of both the ASAPS and ICEPAC models for monthly median propagation, predicted SNR values show large deviations from measured data which indicates that an improvement of these models is required for the African region.

6.1 Summary of the Results

The ionosphere is important for long-distance HF communication, and ionospheric parameters play a big role in HF propagation prediction models. The variations in HF communication performance are directly related to changes in the ionosphere (Stewart, 2008). The HF propagation prediction models (ASAPS and ICEPAC) have many input parameters which may affect the output results.

The recent study done over central Europe by Zolesi *et al.* (2008) during the declining phase of solar cycle 23 (2003-2004) has shown a good performance of the

maximum usable frequency (MUF) for both ASAPS and ICEPAC propagation models. However, the study presented in this thesis was undertaken over the African region during the minimum solar activity period (2008 and 2009).

In this project the validation of these models was undertaken for mostly moderate conditions, $Q_e = 3$. Monthly median HF propagation predictions were presented for both ASAPS and ICEPAC models, while the daily propagation predictions were presented for the ICEPAC model only.

The monthly median HF propagation results show that the ASAPS model did not perform effectively for the three months selected. The inability of ASAPS to predict HF propagation conditions compared to the measured data for the two paths considered may be attributed to several factors, including different types of antennas used. The transmitter and receiver antennas used in ASAPS and the IBP monitor stations differ and this accounts for the major differences between the measured and predicted SNR values. In order to try and harmonise predicted and measured SNR values, a suggestion was made that a correction factor for the calculated gain of the antenna (IBP) be subtracted from each predicted SNR value. Due to various constraints including costs involved, this suggestion was not met and therefore it is recommended that in the future a proper comparison be made between ASAPS derived prediction values and measured data. The ASAPS version used in this project did not contain the coefficients parameter.

Compared to the measured data, the ICEPAC prediction values reveal a more accurate performance for daily HF propagation conditions as opposed to monthly median results over the African region. However, according to Zolesi *et al.* (2008), ICEPAC and other HF propagation prediction models describe long-term variations as derived from the solar cycle, but do not necessarily follow the day-to-day changes in HF propagation channel characteristics. Therefore, the daily prediction values of ICEPAC may not be the only consideration that provide a general overview of its performance. The ability of the ICEPAC model to predict daily HF propagation conditions over Africa is a positive result since there is a need for a model that provides accurate predictions for this region. Therefore, it has been suggested that further investigation be done by validating the ICEPAC model with

more data under all conditions.

As mentioned before, an improvement of ICEPAC for long-term predictions, such as monthly median, is needed. Lane (2005) recommends that ICEPAC should be used with caution in order to generate correct predictions. Lane (2005) also stated that "there is a reason to feel that the major changes in ionospheric modelling in ICEPAC may require a new correlation with measurements in order to correct the needed distribution of transmission loss". Given that ICEPAC's performance is still lacking over the African region, a step to adapt it by incorporating data from our region of interest may be useful for future predictions. The ICEPAC and ASAPS models have, in their development, used their own ionospheric models, which do not necessarily include ionospheric behaviour over Africa. The ICEPAC model in particular does not allow for the updating of coefficients to take into account the African region, nor for the insertion of Africa's own ionosphere.

6.2 Future Work

This attempt at validation of HF propagation models covered only two paths in the whole African region and may not be enough to assess the performance of the models and make very objective conclusions. It is therefore recommended that as many stations as possible within the African region be used for a wider area coverage in order to make a better judgement about the model's performance. The installation of more beacon transmitters is required to make a comprehensive validation of HF propagation models over the African region.

The validation of HF propagation models was performed for a short period of minimum solar activity. ASAPS and ICEPAC are long-term prediction models (Zolesi *et al.*, 2008) and in this thesis only seasonal variation was taken into account. Investigation of these HF propagation models during high solar activity periods is required to assess their performance under all conditions. This requires the continuous archiving of data covering at least an entire solar cycle.

An improvement of the ICEPAC model can be achieved by changing the coefficients or adding more ionospheric data obtained from the African region in the coeffi-

cients. However, the coefficients contain the structure of the ionosphere and are hard wired into the code and this makes it difficult to change the ionospheric configuration to suit a different location. Changing coefficients or having the flexiblity to include our own ionosphere may improve the performance of HF propagation modelling over the African region.

In conclusion, there is still a huge amount of work to be done in trying to find the most accurate HF propagation prediction tool. After this validation trial, it can be concluded that the development of a new HF propagation prediction tool for the African region or adapting one of the investigated models may be considered as an option to ensure more accurate predictions over this region.

References

Advanced Stand Alone Prediction System (ASAPS) Manual, *IPS Radio and Space Services*, Australian Government, Bereau of Meteorology, 2008.

Bothmer V. and Daglis I.A., *Space Weather: Physics and Effects*, Praxis Publishing Ltd, Chichester, UK, 2007.

Brown B., "HF Propagation tutorial", http://www.astrosurf.com/luxorion/qsl-hf-tutorial-nm7m3.htm, retrieved September, 2009.

Carr J.J., "Directional or Omnidirectional Antenna?", Radio Tech-Notes, Joe Carr's Receiving Antenna Handbook, Hightext, 1993.

Carr J.J., *Antenna Toolkit*, Newnes, England, second edition, 2001a.

Carr J.J., *Practical Antenna Handbook*, McGraw-Hill Professional, United States of America, fourth edition, 2001b.

Caruana J., "New Service Developments at IPS Radio and Space Services", IPS Radio and Space Services, 2009.

Coetzee P.J., "Application of the IRI in Southern Africa", *Advances in Space Research*, **34**(9), pp. 2075–2079, 2004.

Daglis I.A., *Effects of Space Weather on Technology Infrastructure*, Kluwer Academic Publishers, Netherlands, 2004.

De Canck M.H., "Faros 1.0. A New NCDXF/IARU Beacon Monitoring Program - Part 2", AntenneX Issue No. 112, August, 2006a.

De Canck M.H., "Propagation Prediction Programs Explained - Part 20", AntenneX Issue No. 109, May, 2006b.

Dennison M. and Fielding J., *Radio Communication Handbook*, Radio Society of Great Britain, Britain, 2007.

Doberstein D., "Correlation, Correlation Receivers, Sliding Correlator's and the PLL Correlator", retrieved from http://www.dkdinst.com/articles/Cor_art.html on November, 2009.

Goodman J.M., *Space Weather & Telecommunications*, Springer, New York, USA, 2005.

Gulyaeva T., "Linkage of the ionospheric peak electron density and height deduced from the topside sounding data", *Advances in Space Research*, **43**(11), pp. 1794–1799, 2009.

Habarulema J.B., McKinnell L.A. and Opperman B.D.L., "A recurrent neural network approach to quantitatively studying solar wind effects on TEC derived from GPS; preliminary results", *Annales Geophysicae*, **27**(5), pp. 2111–2125, 2009.

Haselgrove J., "Ray Theory and a New Method for Ray Tracing", *Report of the Physical Society Conference*, The physics of the ionosphere, Cavedish Laboratory, Cambridge, UK, 1954.

Hutchinson C.L., *The ARRL Handbook for the Radio Amateur*, American Radio Relay League, USA, 1985.

International Telecommunication Union Recommendation: ITU-R, "Radio noise", Recommendation ITU-R P.372-9, 2007.

Lane G., "Review of the High Frequency Ionospheric Communications Enhanced Profile Analysis and Circuit (ICEPAC) Prediction Program", Preprint paper 2B-1, Ionospheric Effects Symposium, Alexandria VA USA, May 3-5, 2005.

Laster C., *The Beginner's Handbook of Amateur Radio*, McGraw-Hill companies, New York, USA, fourth edition, 2000.

Luetzelschwab C., "An Introductory Tutorial to VOACAP", retrieved from www.arrl.org/tis/info/pdf/Voacap.pdf, April, 2004.

McKinnell L.A., *A Neural Network Based Ionospheric Model for the Bottomside Electron Density Profile over Grahamstown South Africa*, Ph.D. thesis, Rhodes University, Grahamstown, South Africa, 2002.

McNamara L.F., *The ionosphere: Communications, Surveillance, and Direction Finding*, Krieger publishing company, Malabar, Florida, 1991.

McNamara L.F., Decker D.T., Welsh J.A. and Cole D.G., "Validation of the Utah State University Global Assimilation of Ionospheric Measurements (GAIM) model predictions of the maximum usable frequency for a 3000 km circuit", *Radio Science*, **42**, pp. 1245–1247, 2007.

Milan S.E., Yeoman T.K., Lester M., Thomas E.C. and Jones T.B., " Initial backscatter occurrence statistics from the CUTLASS HF radars", *Annales Geophysicae*, **71**, pp. 703–718, 1997.

Mudzingwa C., *A real time HF beacon monitoring station for South Africa*, Master's thesis, Rhodes University, Grahamstown, South Africa, 2009.

Pearson F., *Map Projections: Theory and Applications*, CRC Press, Florida, USA, 1990.

Prölss G.W., *Physics of the Earth's Space Environment*, Springer, Berlin Heidelberg, New York, 2004.

Sheikh N.M., *Introduction of Satellite Data into F-2 Layer Models*, Ph.D. thesis, University of Engineering & Technology, Lahore, Pakistan, 1979.

Sizun H., *Radio Wave Propagation for Telecommunication Applications*, Springer, New York, USA, 2004.

Stewart F.G., *Ionospheric Communications Enhanced Profile Analysis & Circuit (ICEPAC) Prediction Program*, Technical Manual, available for download on the internet at http://elbert.its.bldrdoc.gov/pc_hf/hfwin32.html, 2008.

Tascione T.F., Kroehl H.W., Creiger R., Freeman J.W., Jr., Wolf R.A., Spiro R.W., Hilmer R.V., Shade J.W. and Hausman B.A., "New Ionospheric and Magnetospheric Specification Models", *Radio Science*, **33**(3), pp. 211–222, 1988.

Thrane E.V., Jodalen V., Stewart F., Saleem D. and Katan J., "Study of measured and predicted reliability of the ionospheric HF communication channel at high latitudes", *Radio Science*, **29**(5), pp. 1293–1309, 1994.

Zolesi B., Fontana G., Perrone L., Pietrella M., Romano V., Tutone G., Belehaki A., Tsagouri I., Kouris S., Vallianatos F., Makris J.P. and Angling M.J., "A new campaign for oblique-incidence ionospheric sounding over Europe and its data application", *Journal of Atmospheric and Solar-Terrestrial Physics*, **70**, pp. 854–865, 2008.